Bottom Friction for Wind Sea and Swell in Extreme Depth-Limited Situations

NANNE WEBER

Royal Netherlands Meteorological Institute (KNMI), De Bilt, The Netherlands

(Manuscript received 16 August 1989, in final form 13 July 1990)

ABSTRACT

A severe depth-limited storm and a case of extreme swell, which both occurred in the southern North Sea, are hindcasted with a regional version of the third-generation WAM model. This is done using different expressions for the bottom-dissipation source term: an empirical expression, the Hasselmann and Collins drag-law expression and an expression based on the eddy-viscosity concept. An efficient approximation to this eddy-viscosity model is presented, which is easy to compute and which yields accurate results. It is proposed to take a constant roughness value $k_N = 4$ cm in this model, which corresponds to small sand ripples. The validity of this assumption is investigated. The hindcast results are compared with measurements from different stations and an estimate is made of the influence of the tide on the wave dissipation in the southern North Sea. The eddy-viscosity model is found to be a promising alternative to the empirical expression, which is used now in the WAM model.

1. Introduction

Shallow-water wave forecasting models have to take finite-depth effects into account. Different models do this in different ways. Depth appears partly because of the depth dependence of the dispersion relation (refraction, shoaling) and partly because of the direct influence of the bottom. Surface gravity waves with wave lengths, which are long compared to the water depth, give rise to orbital velocities that extend down to the sea floor. This causes an interaction between the waves and the bottom.

The evolution of the wave spectrum is given by the energy-balance equation, which describes the local change of the spectrum due to advection, refraction, and a number of source terms. These terms are input of energy by the wind, dissipation by whitecapping, and transfer of energy by the resonant four-wave interactions. For shallow water there is also a source term that describes the wave-bottom interaction. In addition to the direct bottom effects, the resonant interactions are modified in shallow water and the dissipation by whitecapping is possibly enhanced due to increased wave steepness.

From measurements it is known that there is a depth-dependent reduction of the total energy of the wave field. This can be ascribed to bottom dissipation and possibly to an enhanced dissipation at the surface. There are many different approaches to the modeling of this energy reduction, which reflects how widely opinions diverge on which effect is the dominant underlying physical mechanism. Recently an intercomparison was made (SWIM 1985) of three operational shallow-water wave models that make different assumptions to model finite-depth effects. This showed large differences in predicted results.

The observed energy reduction in shallow water has been modeled by assuming a depth-dependent self-similar spectral shape (Bouws et al. 1985) or by the use of an explicit bottom dissipation source term. Possible wave–bottom interaction mechanisms are: friction, percolation, motion of a soft, muddy bottom, and scattering on bottom irregularities. An estimate of the order of magnitude of these mechanisms as a function of the bottom conditions has been given by Shemdin et al. (1978). They found that friction dominates for fine sand or when sand ripples are present, which is often the case for continental shelf conditions (Komar et al. 1972; Amos et al. 1988). Friction is therefore the most likely wave–bottom interaction mechanism for continental shelves.

An expression for the energy dissipation due to bottom friction, which is based on a quadratic drag law for the bottom stress, was derived by Hasselmann and Collins (1968). Collins (1972) gave an approximation for this expression that is easier to compute. Hasselmann and Collins formulated their theory for a combined wave–current flow. Application of their expression to the JONSWAP measurements of swell dissipation (JONSWAP 1973) led however to contradictory results. Although their theory predicts a pronounced influence of the tidal current on the wave dissipation, the tidal signal was not visible in the data. An alternative for the Hasselmann and Collins expression is the empirical dissipation expression, which was derived

Corresponding author address: Dr. S. L. Weber, Royal Netherlands Meteorological Institute, P.O. Box 201, 3730 AE De Bilt, The Netherlands.

from the JONSWAP measurements. The dissipation coefficient, which occurs in this expression, varies over two orders of magnitude in JONSWAP. The use of this empirical expression (with the mean JONSWAP value for the dissipation coefficient) has nevertheless proved to be successful for swell prediction in the southern North Sea.

To get more insight in the relative importance of the different source terms, the energy balance equation was solved numerically in Weber (1988) for an idealized situation and for different water depths. This was done with explicit calculations of the resonant interactions. It was assumed that friction is the dominant wave–bottom interaction mechanism and the empirical dissipation expression was used with the mean value for the dissipation coefficient. It was found that the transfer of energy to the lower frequencies by the resonant interactions is balanced by the increasing bottom dissipation, soon after the waves have grown long enough so that they can feel the bottom. At this stage the transfer rate is small compared to the earlier stages of wave growth. An equilibrium is then reached, while there is still considerable input of energy by the wind in the energy containing range of the spectrum. The mean JONSWAP dissipation coefficient resulted in unrealistic high energy levels for the lower water depths.

A qualitatively similar balance between the source terms was found by Bouws and Komen (1983) in their analysis of a severe depth-limited storm. This so-called Texel storm was characterized by approximately stationary wind conditions. Bouws and Komen also used the empirical JONSWAP expression for the bottom dissipation. To obtain an equilibrium they had to take a value for the dissipation coefficient that is almost twice the mean JONSWAP value.

An analysis of the wave–bottom interaction is needed to improve on the expression for the bottom dissipation and to explain the wide scatter in the dissipation coefficient. The wave energy loss due to friction in the turbulent bottom boundary layer depends on the bottom stress (Kajiura 1968) and thus on the parameterization of the bottom stress. The most simple parameterization, a drag law, gave unsatisfactory results in the JONSWAP analysis. A more sophisticated parameterization for the turbulent stress, which still allows for an analytical solution of the boundary layer equations, is the linear eddy-viscosity model. The bottom dissipation expression, which results from this model, differs significantly from the drag-law expression. In Weber (1989) an eddy-viscosity dissipation expression is derived for the random wave case and the differences between the drag-law and the eddy-viscosity expressions are investigated theoretically. The stochastic characteristics of the stress parameterization were found to determine the form of the dissipation expression.

In the present study the two expressions will be compared by using them in a wave model. An efficient approximation to the eddy-viscosity expression is presented, which is much easier to compute and which yields the same results as the full expression to within 3%.

The drag-law and the eddy-viscosity expressions are similar to the JONSWAP expression, but they contain a dissipation coefficient that explicitly depends on the wave spectrum, the water depth and the bottom roughness. The drag-law expression is proportional to a drag coefficient, which has to be determined experimentally. The eddy-viscosity model is more fundamental in the sense that it does not contain free parameters. However, the dissipation coefficient depends explicitly on the bottom roughness. In theory the roughness length is determined by the flow field and the sediment properties. The complicated interaction between a wave spectrum and the sediment is not yet fully understood, so that in practice the roughness value is often unknown.

Drag-law dissipation expressions have been used before in wave models. The BMO model (SWIM 1985) and Graber and Madsen (1988) both use Collins' approximation. In BMO the drag coefficient is taken as a constant, while Graber and Madsen investigated the effect of different values for this coefficient on growth curves for idealized situations. Cavaleri et al. (1989) compared the full Hasselmann and Collins expression with the empirical JONSWAP expression both for idealized situations and for actual storms. The eddy-viscosity dissipation has not been used before in a wave model. In the present study this expression is applied assuming a constant value of 4 cm for the roughness length, which corresponds to small sand ripples.

The eddy-viscosity and the drag-law dissipation coefficient are tested in the present paper for a severe depth-limited storm (the Texel storm) and for a case of extreme swell. The hindcasts were made using a regional version of the third-generation WAM model (WAMDI group 1988). The hindcast results are compared with measurements from different stations. An estimate is made of the strength of the wave–current interaction in the turbulent bottom boundary layer and the validity of the roughness value used is investigated.

2. General form of the bottom-friction source term

An empirical expression for the spectral bottom-dissipation source term is

$$S_{\text{bot}}(\mathbf{k}) = -C \frac{k}{\sinh 2kh} F(\mathbf{k}) \qquad (2.1)$$

where C is a dissipation coefficient with the dimension of a velocity, $F(\mathbf{k})$ is the energy-density spectrum and $\mathbf{k} = (k_1, k_2) = (k\cos\theta, k\sin\theta)$ is the wavenumber with modulus k and direction θ. The frequency f (radian frequency ω) is related to k and to the water depth h by the dispersion relation: $2\pi f = \omega = (gk$

$\times \tanh kh)^{1/2}$; g is the gravitational acceleration. The minimum of the bottom dissipation function lies slightly below the peak frequency because of the hyperbolic sine in (2.1).

This expression was proposed in JONSWAP for the dissipation of swell in situations where the wave orbital velocities at the bottom are small compared to the tidal velocities. This need not be true for wind sea during a storm event. The dissipation coefficient was found to vary over two orders of magnitude, with a mean value $C = 0.0077$ m s^{-1}. (The coefficient Γ used in JONSWAP is related to C by: $C = 2\Gamma/g$). No correlation was found with the tidal velocity or phase, wind speed, wave energy flux, or wave frequency.

In the next two sections expressions for C in terms of $F(\mathbf{k})$, h, and the bottom roughness will be given, which can be derived assuming a certain parameterization for the turbulent stress in the bottom boundary layer. If the boundary layer thickness is small compared to a horizontal length scale, say, a wave length, the boundary layer can be treated as a correction to the inviscid, nonturbulent outer layer. The boundary layer regime is determined by the bottom roughness and by the known (horizontal) free stream velocity at the top of the boundary layer $\mathbf{U} = (U_1, U_2, 0)$, which is given by ($i = 1, 2$)

$$U_i = \sum_{\mathbf{k}} \frac{k_i}{k} \tilde{U}_{\mathbf{k}} + \text{c.c.} \tag{2.2}$$

with

$$\tilde{U}_{\mathbf{k}} = \frac{1}{2} A_{\mathbf{k}} \frac{\omega}{\sinh kh} e^{i(\mathbf{k}\cdot\mathbf{x}-\omega t)}.$$

Here $A_{\mathbf{k}}$ is the random wave amplitude, $\mathbf{x}$ is the horizontal position coordinate, and t is time; $\mathbf{U}$ is found from potential wave theory (see e.g., Phillips 1980). Mean currents are neglected in the parameterizations; their effect will be discussed briefly in section 7.

3. The dissipation expression based on the eddy-viscosity model

An expression for the spectral energy dissipation due to friction in the turbulent bottom boundary layer, which is based on the eddy-viscosity model, is presented in Weber (1989). The derivation is summarized in appendix A. This expression has the form (2.1), with C a function of the average friction velocity u^*, the bottom roughness, and the wave frequency. The friction velocity u^* is a priori unknown in the eddy-viscosity model; u^* can be determined from the boundary-layer flow and the bottom roughness. In practice this is done iteratively. In this section an approximation is derived to the original iteration. This yields an expression for the dissipation coefficient in terms of the bottom roughness and of the free stream velocity at the top of the boundary layer. The approximate iteration scheme gives accurate results and is more efficient in terms of computing time. A value is proposed for the roughness length and an estimate is made of the dependence of the dissipation coefficient on the water depth and the wind friction velocity for the fully grown sea state.

a. Summary of the eddy-viscosity model

First the main features of the eddy-viscosity model will be described for the random wave bottom boundary layer (see also appendix A). In the eddy-viscosity model the turbulent shear stress is parameterized in analogy with the viscous stress, with the coefficient of molecular viscosity replaced by a turbulent eddy-viscosity coefficient. The eddy-viscosity coefficient is proportional to the distance from the bottom and to the friction velocity u^*, which is defined as

$$u^* = \langle \tau_0^{1/2} \rangle \tag{3.1}$$

with $\tau_0^{1/2} = \{\tau_1^2(y_0) + \tau_2^2(y_0)\}^{1/4}$. Here $\boldsymbol{\tau} = (\tau_1, \tau_2)$ is the turbulent shear stress and $\langle \cdot \rangle$ stands for ensemble averaging. For notational convenience the water density ρ is absorbed in the stress in the remainder of this paper, and $y_0 = -h + k_N/30$ denotes the theoretical bottom level, where the velocity is taken to be zero in case of a hydrodynamically rough bottom. This theoretical zero level parameterizes the small-scale flow around the roughness elements on the bottom. Any roughness can be correlated with its equivalent Nikuradse sand roughness (see e.g., Schlichting 1955), which is denoted here by k_N. The roughness length k_N is a function of the magnitude and the spacing of the roughness elements (sand grains, ripples) and has to be determined experimentally.

Solving the boundary layer equations with the eddy-viscosity parameterization yields for the bottom stress:

$$\tau_i(y_0) = u^* \sum_{\mathbf{k}} \frac{k_i}{k} T_{\mathbf{k}}(\xi_0) \tilde{U}_{\mathbf{k}} + \text{c.c.} \tag{3.2}$$

Here $T_{\mathbf{k}}$ is a dimensionless complex function (see appendix A); the complex phase denotes the phase shift $\zeta_{\mathbf{k}}$ between a bottom-stress component and a free stream velocity component; $T_{\mathbf{k}}$ depends on the radian frequency and thus on the wave number through the argument ξ_0. This variable is defined as

$$\xi_0 = \left(\frac{4(y_0 + h)\omega}{\kappa u^*}\right)^{1/2} = \left(\frac{4k_N\omega}{30\kappa u^*}\right)^{1/2}. \tag{3.3}$$

The variable ξ_0 reflects the ratio between the roughness length and the boundary layer thickness, which scales with u^*/ω, and $\kappa = 0.4$ is the von Kármán constant. At a distance $5u^*/\omega$ from the bottom, the velocity deviates less than one percent from the free stream velocity and the stress is reduced to less than three percent of its bottom value. The boundary layer thickness d can therefore be taken as $d = 5u^*/\omega$.

The stress components are, in a statistical sense, lin-

ear functions of the free stream velocity, as u^* is an average quantity. This means that τ_1 and τ_2 are jointly Gaussian. Note that a doubling of the velocity does not result in a doubling of the stress. In this sense the stress is not linear. The friction velocity is defined in terms of the bottom stress, which again depends on the free stream velocity as well as on the friction velocity itself, so that the relationship is highly nonlinear.

Making use of the Gaussian distribution function of τ, the definition (3.1) of the friction velocity can be rewritten as

$$u^* = \sigma_{11}^{1/2} F_3(A). \tag{3.4}$$

Note that F_3 is given in appendix A. The argument A is given by

$$A = 1 - \sigma_{22}/\sigma_{11}. \tag{3.5}$$

The bottom stress variances normalized by u^*, are given by $(i, j = 1, 2)$

$$\sigma_{ij} = \left\langle \frac{\tau_i \tau_j}{u^{*2}} \right\rangle = \int_{\mathbf{k}} \frac{k_i k_j}{k^2} T_{\mathbf{k}}(\xi_0) T_{\mathbf{k}}^*(\xi_0) \frac{\omega^2}{\sinh^2 kh} F(\mathbf{k}) d\mathbf{k}. \tag{3.6}$$

In (3.4) and (3.5), σ_{11} and σ_{22} are calculated relative to a coordinate system that has $\sigma_{12} = 0$ and $\sigma_{22} \leq \sigma_{11}$. This coordinate system is obtained from the given coordinate system by rotating through an angle ϕ (see appendix A) with ϕ the main axis of the turbulent stress spectrum. The argument A is a measure for the directional spread of the bottom stress spectrum. In case of a one-dimensional surface elevation spectrum $A = 1$; for an isotropic spectrum $A = 0$. Generally A takes values between $\frac{2}{3}$ ($a \cos^2$ – angular distribution) and 1 (unidirectional case).

The friction velocity u^* has to be determined iteratively, as the bottom stress variances σ_{ij} depend on u^* through the argument ξ_0 of $T_{\mathbf{k}} T_{\mathbf{k}}^*$. The surface elevation spectrum $F(\mathbf{k})$, the water depth h, and the bottom roughness k_N define the iteration. A unique solution always exists and usually less than ten iteration steps are sufficient.

The dissipation coefficient, which can be derived from the eddy-viscosity model, is given by

$$C_{\text{eddy}} = u^* \{ T_{\mathbf{k}}(\xi_0) + T_{\mathbf{k}}^*(\xi_0) \}. \tag{3.7}$$

Here C_{eddy} depends on the wave spectrum $F(\mathbf{k})$, the water depth h, and the bottom roughness k_N through u^*, as well as on the radian frequency through ξ_0. The proper nondimensional quantity to use is evidently $T_{\mathbf{k}} + T_{\mathbf{k}}^*$, but to maintain the similarity with the empirical JONSWAP expression (2.1), the dimensional coefficient C_{eddy} is used here. Substituting (3.7) in (2.1) it is seen that the dissipation time scale is $(u^* k)^{-1}$.

b. The approximate eddy-viscosity dissipation coefficient

The expression (3.7) does not give insight into the dependence of the dissipation coefficient on $F(\mathbf{k})$, h and k_N, because the friction velocity cannot be expressed explicitly in terms of these quantities. Furthermore, (3.7) is time-consuming to compute. Therefore, an approximation is introduced in the iteration scheme for u^* that yields results close to the exact ones. This approximation allows for a numerical determination of u^* in terms of one dimensionless parameter that characterizes the boundary-layer regime.

The normalized bottom stress variances σ_{ij} are slowly varying functions of the argument ξ_0 of $T_{\mathbf{k}} T_{\mathbf{k}}^*$. This suggests replacing ξ_0 in (3.6) by ξ_0^p, with

$$\xi_0^p = \left(\frac{4 k_N \omega_p}{30 \kappa u^*} \right)^{1/2} \tag{3.8}$$

where ω_p is the peak radian frequency of the surface elevation spectrum. The σ_{ij} can now be expressed as

$$\sigma_{ij} = T_{\mathbf{k}}(\xi_0^p) T_{\mathbf{k}}^*(\xi_0^p) \int_{\mathbf{k}} \frac{k_i k_j}{k^2} \frac{\omega^2}{\sinh^2 kh} F(\mathbf{k}) d\mathbf{k} = T_{\mathbf{k}}(\xi_0^p) T_{\mathbf{k}}^*(\xi_0^p) \langle U_i U_j \rangle. \tag{3.9}$$

The bottom velocity variances $\langle U_i U_j \rangle$ can be determined directly from the surface elevation spectrum and the water depth. It is to be expected that the approximation is more accurate for narrow spectra than for broad spectra. The bottom velocity spectrum is generally very narrow, as the high frequency components mostly do not extend down to the sea floor. For double-peaked spectra that have peaks which appear both in the bottom velocity spectrum, the approximation should be modified to account for the double-peakedness.

Substitution of (3.9) in (3.4) yields

$$u^* = \{ T_{\mathbf{k}}(\xi_0^p) T_{\mathbf{k}}^*(\xi_0^p) \}^{1/2} \langle U_1^2 \rangle^{1/2} F_3(A) \tag{3.10}$$

with

$$A = 1 - \langle U_2^2 \rangle / \langle U_1^2 \rangle. \tag{3.11}$$

This defines the friction velocity u^* in terms of ω_p, k_N, and $\langle U_1^2 \rangle^{1/2} F_3(A)$. These can be combined to one dimensionless parameter, which will be denoted as z_b:

$$z_b = \frac{k_N \omega_p}{U_b} \tag{3.12}$$

with

$$U_b = \langle U_1^2 \rangle^{1/2} F_3(A).$$

In (3.12) the bottom roughness is scaled with the exterior length scale U_b/ω_p, which can be interpreted as a scale for the excursion amplitude at the top of the bottom boundary layer. This length scale replaces the interior scale u^*/ω (the boundary layer thickness),

which appeared in (3.3), and z_b replaces ξ_0 as a basic parameter for the bottom boundary layer.

The parameter z_b has a one-to-one correspondence to $\xi_0{}^p$; from (3.10) it follows with the use of (3.8) that

$$z_b = \frac{k_N \omega_p}{U_b} = \frac{30\kappa}{4} (\xi_0{}^p)^2 \{ T_k(\xi_0{}^p) T_k^*(\xi_0{}^p) \}^{1/2}. \quad (3.13)$$

The parameter $\xi_0{}^p$ can be found numerically by inversion of (3.13) if z_b is given.

Various quantities, which are of importance in the eddy-viscosity model, can be expressed in terms of z_b using (3.13). The friction velocity u^*, made dimensionless with U_b, and the phase shift ζ are given in Fig. 1. Both are slowly varying functions of z_b. For increasing z_b, u^* takes values that are increasing fractions of U_b, and ζ decreases. The stress components are thus seen to be 150° to 170° in advance of the velocity components, so that a stress component is at its maximum when the corresponding free stream velocity component decelerates. There is an adverse pressure gradient during decelerating flow, which enhances instability according to the point-of-inflexion criterion (Schlichting 1955). An increase in turbulence intensity is therefore to be expected for decelerating free stream velocity. Turbulent bursts at flow deceleration were also found experimentally by Hino et al. (1983).

The eddy-viscosity dissipation coefficient can now be approximated by substitution of (3.10) in (3.7):

$$\tilde{C}_{eddy} = -2 \cos(\zeta) T_k(\xi_0{}^p) T_k^*(\xi_0{}^p) \times \langle U_1{}^2 \rangle^{1/2} F_3(A). \quad (3.14)$$

An explicit algebraic expression in terms of z_b, which fits the curve defined by (3.14) closely, is given by

$$\tilde{C}_{eddy} = \exp(-8.34 + 6.34 z_b{}^{0.08}) U_b. \quad (3.15)$$

This fit was obtained using a standard curve-fitting technique. In the range $10^{-4} < z_b < 1$, equation (3.15) fits the curve defined by (3.14) to an accuracy of better than 3%. The approximate dissipation coefficient (3.15), made dimensionless with U_b, is given in Fig. 2. For a number of test spectra, water depths, and roughness lengths (3.15) was found to yield values for the dissipation coefficient, which are within 3% of the values obtained from the original expression (3.7) with the friction velocity determined from the iteration scheme (3.4)–(3.6). The values obtained for these test cases from the original expression (3.7) are also indicated in Fig. 2.

The approximate dissipation coefficient (3.15) will be used in the hindcasts. This expression takes only three times as much CPU time as the empirical expression (2.1), while the full expression (3.7) takes four times as much CPU time as (2.1). The gain seems relatively small. The approximate expression (3.15) can, however, be further simplified, using a numerically determined expression for U_b in terms of the spectral

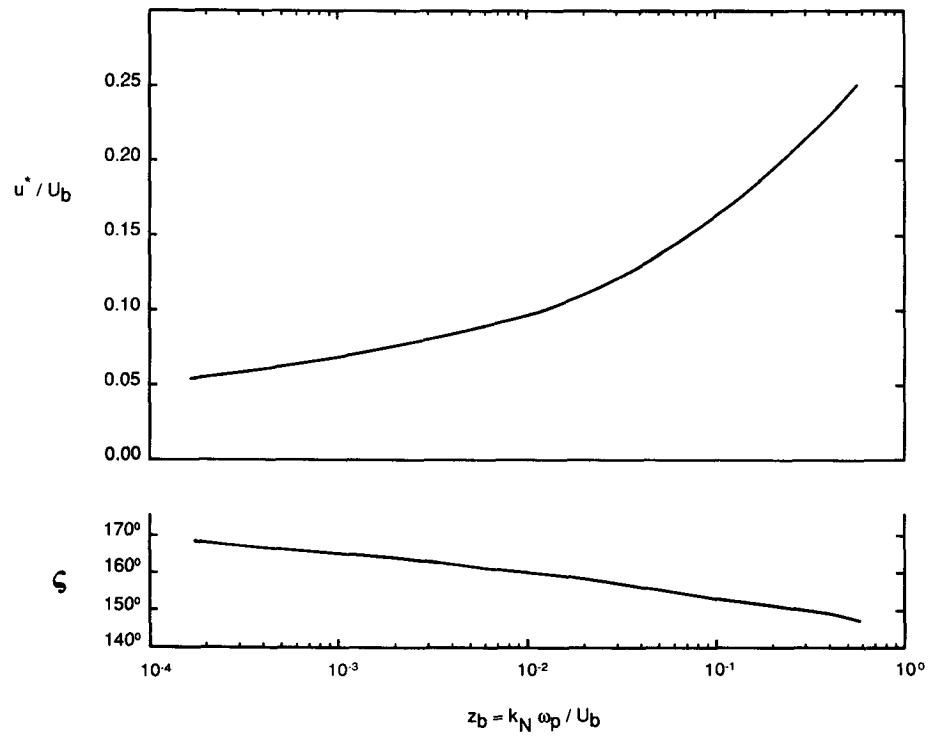

FIG. 1. The friction velocity u^*, made dimensionless with U_b, and the phase shift ζ as functions of the parameter z_b.

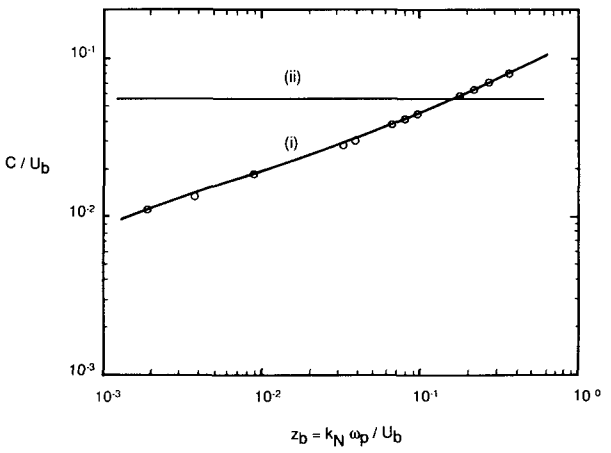

FIG. 2. The dissipation coefficient C, made dimensionless with U_b, as a function of the parameter z_b: (i) the approximate eddy-viscosity expression (3.15). For a number of test cases C/U_b has also been computed from the original expression (3.7), with u^* determined from (3.4)–(3.6); these are denoted by circles. (ii) the drag-law expression (4.2) for the main direction $\theta = \phi$ (and an example directional spread $A = \frac{2}{3}$); $c_D = 0.015$. See section 4.

parameters (see section 3.d). This results in an expression for the dissipation coefficient in terms of the spectral parameters and the bottom roughness, which hardly takes computing time and which is probably adequate for most operational purposes.

c. *The roughness length*

The eddy-viscosity dissipation coefficient explicitly depends on the roughness length k_N, although the dependence is more on the order of magnitude of k_N than on its precise value. For a flat bottom, k_N is of the order of magnitude of the sand grain diameter D_m ($D_m \sim 0.1$ mm); this, however, yields values for the dissipation coefficient that are much too low to be realistic. If there are sand ripples present, k_N is of the order of magnitude of the ripple height. In this paper a value $k_N = 4$ cm will be used as a first guess. Assuming that k_N is two to four times the ripple height, this corresponds to 1–2 cm ripples. The validity of this assumption will be investigated in section 8.

d. *The dissipation coefficient for the fully grown sea state*

Now that the value of the roughness length is fixed, the dissipation coefficient (3.15) depends only on the wave field (through U_b and ω_p). For the idealized situation of a constant offshore wind and a straight coast line, the significant wave height H_s and ω_p can be related to the fetch, the water depth, and the wind (friction) velocity. The dissipation coefficient can then be related to these variables if U_b is expressed in terms of H_s and ω_p.

In appendix B it is shown that for a JONSWAP spectrum the characteristic velocity U_b can be expressed as

$$U_b = 0.2\omega_p H_s Q(k_p h) \tag{3.16}$$

where k_p is the wavenumber, which corresponds to the peak frequency, and Q is determined numerically from the relative water depth $k_p h$ and the spectral form $F(f)$. Substituting this relation in (3.15), it follows that

$$\tilde{C}_{\text{eddy}} = \tilde{C}_{\text{eddy}}\left(\frac{k_N}{H_s Q(k_p h)}, \omega_p H_s Q(k_p h)\right). \tag{3.17}$$

The range of the eddy-viscosity dissipation coefficient and the dependence on the fetch, the wind friction velocity, and the water depth can be estimated from (3.17) applying the empirical CERC (1977) growth curves (see appendix B). The dissipation coefficient is found to increase with increasing fetch, until an asymptotic value is reached. The asymptotic values are shown in Fig. 3 as a function of the wind friction velocity and the water depth. The lowest value for C for the different water depths corresponds to $k_p h = 2$, where the waves just start to feel the bottom. The asymptotic

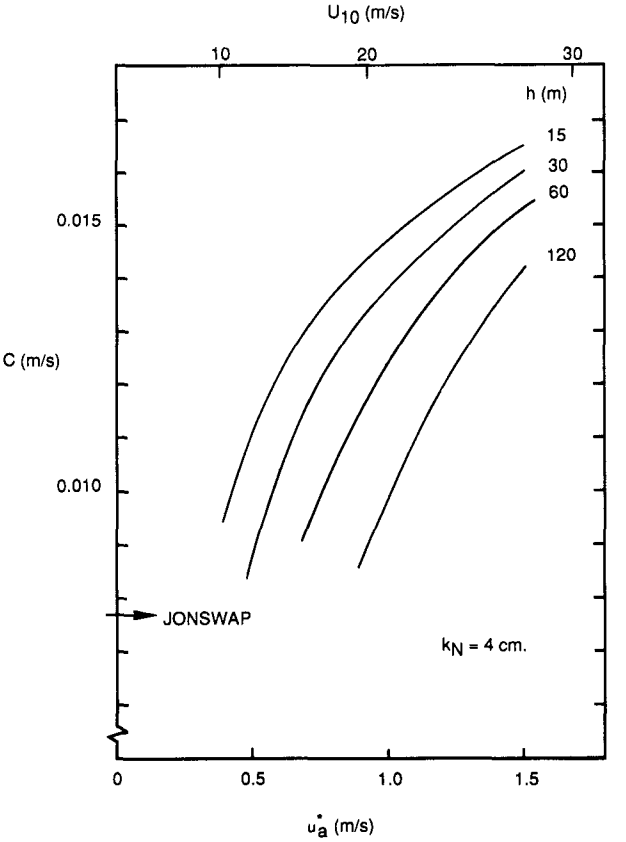

FIG. 3. The asymptotic values for the eddy-viscosity dissipation coefficient as a function of the wind friction velocity u_a^* (the mean wind speed U_{10}) for different water depths h and for $k_N = 4$ cm.

values for C increase for decreasing water depths and for increasing wind speeds. For the range of water depths and wind speeds considered here, the asymptotic values lie between 0.008 and 0.017 m s^{-1}, which is always above the mean JONSWAP value. Only in the earlier stages of wave growth can C obtain lower values.

e. Eddy-viscosity models for oscillatory flow

The eddy-viscosity concept was first applied to the oscillatory boundary layer by Kajiura (1968). Later it was used by Grant and Madsen (1979) and Christofferson and Jonsson (1985) to describe the combined wave–current flow and by Grant and Madsen (1982) to describe the wave-sediment interaction. These models are all formulated for monochromatic waves. Since the present work was completed, Madsen et al. (1989) have also presented an eddy-viscosity dissipation expression for the random wave case.

The present eddy-viscosity model differs from the one given by Madsen et al. in the following respects. A different definition of u^* is used here, which takes the directional distribution of the bottom stress spectrum into account. The influence of the phase shift between the bottom stress and the free stream velocity on the wave energy dissipation is taken into account in the present model. The full expression for the bottom stress is used here, in place of a logarithmic approximation for small k_N/d values. Typically, $k_N/d \sim 0.1$ in the applications considered in the following. Neglect of the phase shift and the use of the logarithmic approximation for k_N/d in this order of magnitude enhances the energy dissipation compared to the present expression.

Madsen et al. approximate the random wave field by an "equivalent" monochromatic wave. In the present paper a similar approximation is made. Madsen et al., however, apply this approximation in an early stage of their calculations and thereby rederive Collins' drag-law dissipation expression. Therefore their expression is only valid for a narrow, single-peaked spectrum. In the present paper the approximation is introduced in the final expression (3.7) to obtain the simpler expression (3.15). The dissipation expression (3.7) is valid for a random wave field in general and can be applied to complicated situations like a turning wind field or swell interacting with wind-sea, where the wave field cannot be easily represented by one wave component.

The final difference lies in the application of the model. Madsen et al. propose to use their expression in combination with a drag coefficient, with the bottom roughness length computed by their wave-sediment model. It is proposed here to use a fixed roughness length. A range of bottom velocities and wave frequencies occur for wind-sea and swell in shallow water, but only a small subset of these give rise to a turbulent bottom boundary layer. This narrows down the range of roughness lengths that are relevant for wave modeling purposes. It is therefore thought that the bottom roughness can be considered as fixed, as long as the chosen roughness value is consistent with the flow and sediment conditions. From Fig. 3 it is clear that a fixed roughness length still allows for a large variability in the dissipation coefficient.

4. Comparison with the drag-law dissipation expression

A quadratic drag law, based on the instantaneous values of the bottom stress and of the free stream velocity at the top of the boundary layer, is

$$\tau_i(y_0) = -c_D U U_i \tag{4.1}$$

with $U = (U_1^2 + U_2^2)^{1/2}$ and c_D a drag coefficient. For monochromatic flows c_D has been determined experimentally as a function of the scaled bottom roughness, see for example, Jonsson (1980).

From (4.1) Hasselmann and Collins (1968) derived an expression for the energy dissipation, which has the form (2.1), but now the dissipation coefficient is given by

$$C_{\text{drag}} = 2c_D\langle U_1^2\rangle^{1/2}\{F_1(A)\cos^2(\theta-\phi) + F_2(A)\sin^2(\theta-\phi)\}. \tag{4.2}$$

The expression given originally by Hasselmann and Collins is rewritten here in a form that facilitates comparison with the eddy-viscosity model, see appendix C for details. The functions F_1 and F_2 are given in appendix C also; the argument A is defined as in (3.11). The angle $\theta - \phi$ is the direction of a wave component relative to the main axis of the bottom velocity spectrum. The drag-law dissipation coefficient takes three times as much CPU time as the empirical JONSWAP expression.

The dissipation coefficient (4.2) depends on the direction of a wave component as well as on the bottom velocity spectrum, because the parameterization (4.1) is stochastically nonlinear in the bottom velocity. This nonlinearity also induces the functions F_1 and F_2 in (4.2), which take larger values than the analogous function F_3, which occurs in the eddy-viscosity expression.

From a limited number of numerical hindcasts, Hasselmann and Collins estimated that c_D could be taken as constant, with $c_D = 0.015$. This value will be used in the following. In Fig. 2, C_{drag}, made dimensionless with U_b, is depicted for the main direction $\theta = \phi$ and for an example directional spread $A = \frac{2}{3}$. It is seen that C_{drag} equals $\tilde{C}_{\text{eddy}}$ for $z_b \sim 0.15$. For smaller values of z_b the drag-law dissipation coefficient is larger than the eddy-viscosity coefficient; for larger values of z_b it is smaller.

5. The Texel storm hindcast

a. Introduction

On 3 January 1976 a severe storm occurred in the southern North Sea, where the water depth is 20–50 m. An extensive description of this storm can be found in Harding and Binding (1978). On 2 January a small but deepening frontal depression had progressed from the Atlantic to the western Highlands of Scotland by 1800 UTC. It continued in an east-northeast direction, then turned east and later southeast to reach its lowest pressure (963 mb) at 0300 UTC 3 January. After 0900 the depression turned further south-southeast, and continuing on its track, the depression filled by 2100. The associated gales reaches the Dutch coast by 2100 UTC 2 January, with mean wind speeds of ~25 m s^{-1}, reaching a maximum mean wind speed of 30 m s^{-1} at 0300 UTC 3 January. Wind direction was west, then turned west-northwest at 0600 and had turned again northwest by 1800.

The wind fields for the hindcast are obtained from subjective three-hourly synoptic weather charts, which were carefully reanalyzed and then digitized. The wind was subsequently computed from the pressure values, using the Hesselberg relation (Hesselberg 1915). The calculated wind fields were compared with observations from a number of land and sea stations and no significant differences were found.

There are hourly measurements available of the one-dimensional frequency spectrum from Texel (53°2′N, 4°17′E; local depth is ~30 m) for the period 0000 to 2100 UTC 3 January. Three-hourly averages are used here. Texel is the most western of the West Frisian Islands, situated in the northern part of the Netherlands, where the storm was at its maximum. There are also six-hourly measurements of the significant wave height and the mean frequency from Eurochannel (52°0′N, 3°41′E) in the southern part of the Netherlands, which was less severely affected. These measurements are for the period 1800 UTC 2 January to 0600 UTC 4 January; at Eurochannel the local depth is ~25 m.

The frequency spectrum $F(f)$ is defined as

$$F(f) = \int_0^{2\pi} F(f, \theta)\, d\theta$$

$$\text{with} \quad F(f, \theta) = \frac{2\pi k}{c_g} F(\mathbf{k}).$$

Here c_g is the magnitude of the group velocity $\mathbf{c}_g = \partial\omega/\partial\mathbf{k}$. Significant wave height H_s, mean frequency $\bar{f}$, and root-mean-square bottom velocity U_{rms} can be obtained from $F(f)$ according to

$$H_s = 4m_0^{1/2}$$

$$\bar{f} = m_0/m_{-1}$$

where

$$m_n = \int_f f^n F(f)\, df$$

$$U_{\text{rms}} = \langle U^2 \rangle^{1/2} = \left\{ \int_f \frac{\omega^2}{\sinh^2 kh} F(f)\, df \right\}^{1/2}.$$

This so-called Texel storm was hindcasted with a regional version of the third-generation WAM model (WAMDI group 1988). The WAM model computes the wave spectrum by integration of the energy-balance equation:

$$\frac{\partial F}{\partial t} + \nabla \cdot \mathbf{c}_g F = S_{\text{tot}} \tag{5.1}$$

where S_{tot} is the total source term consisting of wind input, dissipation by whitecapping, the transfer of energy by the resonant four-wave interactions and, in the case of shallow water, bottom friction. The model behavior is primarily determined by the source terms. Optimization therefore has to come from improving the physical description of wave growth and decay in the model.

WAM runs on a global grid. For the present hindcasts a regional version of WAM (Karssen 1987) was used, which combines the WAM model with the grid and the boundary conditions of the Dutch operational GONO model (Janssen et al. 1984). The GONO grid covers the North Sea area with a grid spacing of 75 km (see Fig. 4). The stations Texel and Eurochannel are indicated in Fig. 4. Refraction is neglected in this version of the WAM model.

For later use, the main features of the source terms used in the WAM model will be briefly described. A more extensive discussion can be found in WAMDI group (1988). The wind input S_{in} is given by

$$S_{\text{in}} = \max\left\{0,\ 0.25 \frac{\rho_a}{\rho}\left(28 \frac{u_a^*}{c_p}\cos\theta_a - 1\right)\right\}\omega F(\mathbf{k}) \tag{5.2}$$

with ρ_a the density of air, u_a^* the wind friction velocity and θ_a the angle between the wind vector and a wave component; $c_p = \omega/k$ is the phase velocity. This expression is based on measurements by Snyder et al. (1981).

For shallow water the dissipation by whitecapping S_{dis} is expressed as

$$S_{\text{dis}} = -2.6\bar{\omega}\frac{k}{\bar{k}}(E\bar{k}^2)^2 F(\mathbf{k}) \tag{5.3}$$

where $E\bar{k}^2$ is the integral wave steepness parameter, with $E = m_0$ the total energy and $\bar{k}$ the mean wavenumber, defined by

$$\bar{k} = \left\{\frac{1}{E}\int_{\mathbf{k}} k^{-1/2} F(\mathbf{k})\, d\mathbf{k}\right\}^{-2}.$$

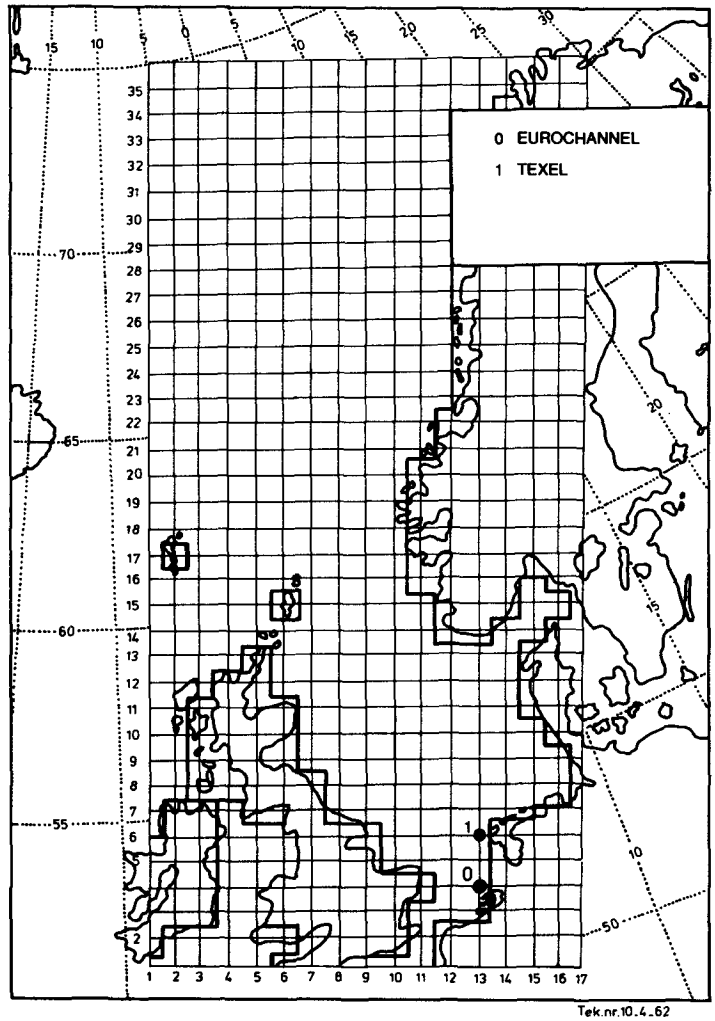

FIG. 4. The GONO computational grid (Δx = 75 km).

The nonlinear transfer S_{nl} is determined by using the discrete interaction-operator parameterization proposed by Hasselmann et al. (1985). This is a deep-water parameterization; the finite-depth case is obtained using a scaling factor R (Hasselmann and Hasselmann 1981), where

$$S_{nl}(k_p h) = R(k_p h) S_{nl}(\infty). \quad (5.4)$$

The scaling factor decreases for decreasing water depths, until a minimum is reached for $k_p h \sim 2$. The factor R then increases again slowly and only becomes large for $k_p h$ smaller than one.

For the bottom-friction source term S_{bot}, the empirical expression (2.1) is used in WAM. For the present hindcasts different expressions for the dissipation coefficient C in S_{bot} were applied:

(J) the mean JONSWAP value $C = 0.0077$ m s^{-1},
(E1) the approximate eddy-viscosity expression (3.15), with $k_N = 4$ cm,
(D2) the drag-law expression (4.2), with $c_D = 0.015$.

To check again on the validity of the approximation made in section 3 to obtain (3.15), a hindcast was also made with the original eddy-viscosity dissipation coefficient (3.7), with the friction velocity determined from the iteration scheme (3.4)–(3.6). The results for H_s, $\bar{f}$ and C from this hindcast were found to lie within 3% of the values from the hindcast with the approximate eddy-viscosity coefficient.

The hindcasts were started at 0000 UTC 1 January. Before the wind increases, $H_s \sim 2$ m and $\bar{f}$ varies between 0.14 and 0.20 Hz. The first effects of the storm are seen in the late afternoon of 2 January, when H_s starts to increase and $\bar{f}$ starts to decrease. At midnight on 3 January the waves have grown so long that bottom friction becomes important. At this point the results of the different hindcasts start to diverge.

b. Hindcast results

In Figs. 5a,b the hindcast results for H_s and $\bar{f}$ are shown together with the measured data for Texel. The empirical expression used conventionally in the WAM model overpredicted H_s by 1–2 m, but performed rather well for $\bar{f}$. Both the eddy-viscosity model and the drag law yield much more realistic results for H_s. However, E1 overpredicts $\bar{f}$ by 0.01 Hz, and D2 overpredicts $\bar{f}$ by 0.015 Hz.

In Fig. 6 the predicted values for the rms bottom velocity are shown, which reflect the foregoing results. The characteristic velocity exhibits the same behavior as the rms velocity (in E1 and in D2 the directional spread $A = 0.75$ so that $U_b = 0.8U_{\text{rms}}$). In Fig. 7a the evolution of z_b is shown for E1 and for D2. The values of the dissipation coefficient are shown in Fig. 7b. In this range of z_b values, D2 yields larger dissipation coefficients than E1 (see also Fig. 2).

In the eddy-viscosity model, $u^* \sim 6$ cm s^{-1} and the phase shift $\zeta \sim 150°$ from 0600 onwards. The boundary layer thickness $d \sim 50$ cm. Both in the eddy-viscosity model and in the drag law the main axis of the bottom stress coincides with the mean wave direction within 5°, which again follows the wind direction within 20°.

Measurements and hindcast results of H_s and $\bar{f}$ for Eurochannel are given in Figs. 8a,b. At Eurochannel J overpredicted H_s and underpredicted $\bar{f}$. The eddy-viscosity model and the drag law yield better results for H_s. The former also performs very well for $\bar{f}$, while the latter overpredicts $\bar{f}$ with 0.005 Hz.

The characteristic velocity $U_b \sim 0.35$ m s^{-1} in E1 from 0600–1800, so that $z_b \sim 0.08$. During this period $U_b \sim 0.3$ m s^{-1} and $z_b \sim 0.1$ in D2. The dissipation coefficients are $C_{\text{eddy}} \sim 0.015$ m s^{-1} and $C_{\text{drag}} \sim 0.019$ m s^{-1} (for the main direction). The boundary layer thickness can be estimated at $d \sim 35$ cm, with $u^* \sim 5$ cm s^{-1}.

Application of the eddy-viscosity expression or the drag-law expression for the dissipation coefficient in S_{bot} clearly results in an enhanced bottom dissipation for the Texelstorm. The nonlinear character of these expressions is apparent here. The dissipation coefficient found in E1 is closest to the value proposed by Bouws and Komen (1983) for the equilibrium phase of this storm. The predicted values for the significant wave height are found to be much improved in E1 and in D2 because of the stronger bottom dissipation. However, D2 overpredicts the mean frequency at both stations, which indicates that the drag-law dissipation coefficient is too high for this storm. At Texel the mean frequency is best predicted by J, while at Eurochannel E1 performs best.

All three hindcasts yield an overprediction of the significant wave height at the beginning of the storm at both stations, see Figs. 5a and 8a. This overprediction sets in when the water can still be considered as deep. The maximum in the significant wave height coincides with a maximum in the mean wind speed. There might be an error in one of the deep-water source terms here. The expression for S_{in} has been derived from measurements that were obtained in low wind conditions. The expression for S_{dis} on the other hand is obtained as an equilibrium solution for a fully developed spectrum. Either one might be incorrect. An alternative source of errors is the input wind field. The wave prediction in a wave model does not depend on the local wind input only; because of propagation effects, previous winds elsewhere are crucial as well. Near the Dutch coast the modeled wind compares satisfactorily with observations (Bouws, private communication), but in the central North Sea the wind field cannot be checked as extensively. An overprediction here might cause the overprediction of sea state closer to the coast.

The mean frequency is best predicted at Texel by J and at Eurochannel by E1, as was mentioned earlier. The marked difference between Texel and Eurochannel is the continuing down shift of $\bar{f}$ at Texel, while $\bar{f}$ remains constant at Eurochannel. I will now describe the energy balance in more detail in order to explain this difference. Then I will investigate qualitative investigation into how the three versions of the wave model react to the overprediction in the significant wave height at the beginning of the storm.

c. The energy balance in finite-depth water

During the first hours of the storm the significant wave height is still increasing. At Texel there is a balance between the energy sources and sinks from 0600 onwards: H_s remains constant, while $\bar{f}$ (and f_p) is still decreasing. Only later does the decrease in $\bar{f}$ stop and an equilibrium is reached for all spectral components. The equilibrium will be assumed from 1200 onwards, because all frequency-dependent quantities reach their equilibrium value at this time. At Eurochannel there is an equilibrium both for H_s and for $\bar{f}$ from 0600 onwards.

The energy balance can be described qualitatively by a number of parameters, which characterize the various terms in the energy-balance equation (5.1). The values of these parameters, obtained from the measured data, are given in Table 1. The inverse wave-age parameter $u_a^*/c_p(f_p)$ characterizes the wind-input source term. Here $c_p(f_p)$ is the phase velocity that corresponds to the peak frequency. The integral wave steepness $E\bar{k}^2$ is important both for the dissipation by whitecapping and for the nonlinear transfer. Both parameters have approximately the same value at Texel and at Eurochannel during the first hours of the storm.

The balance between S_{in}, S_{dis} and S_{nl} is thus similar for Texel and for Eurochannel. As the phase velocities of the waves are much smaller than the wind speed, one expects an increase in significant wave height with a decreasing peak frequency. This situation can be ob-

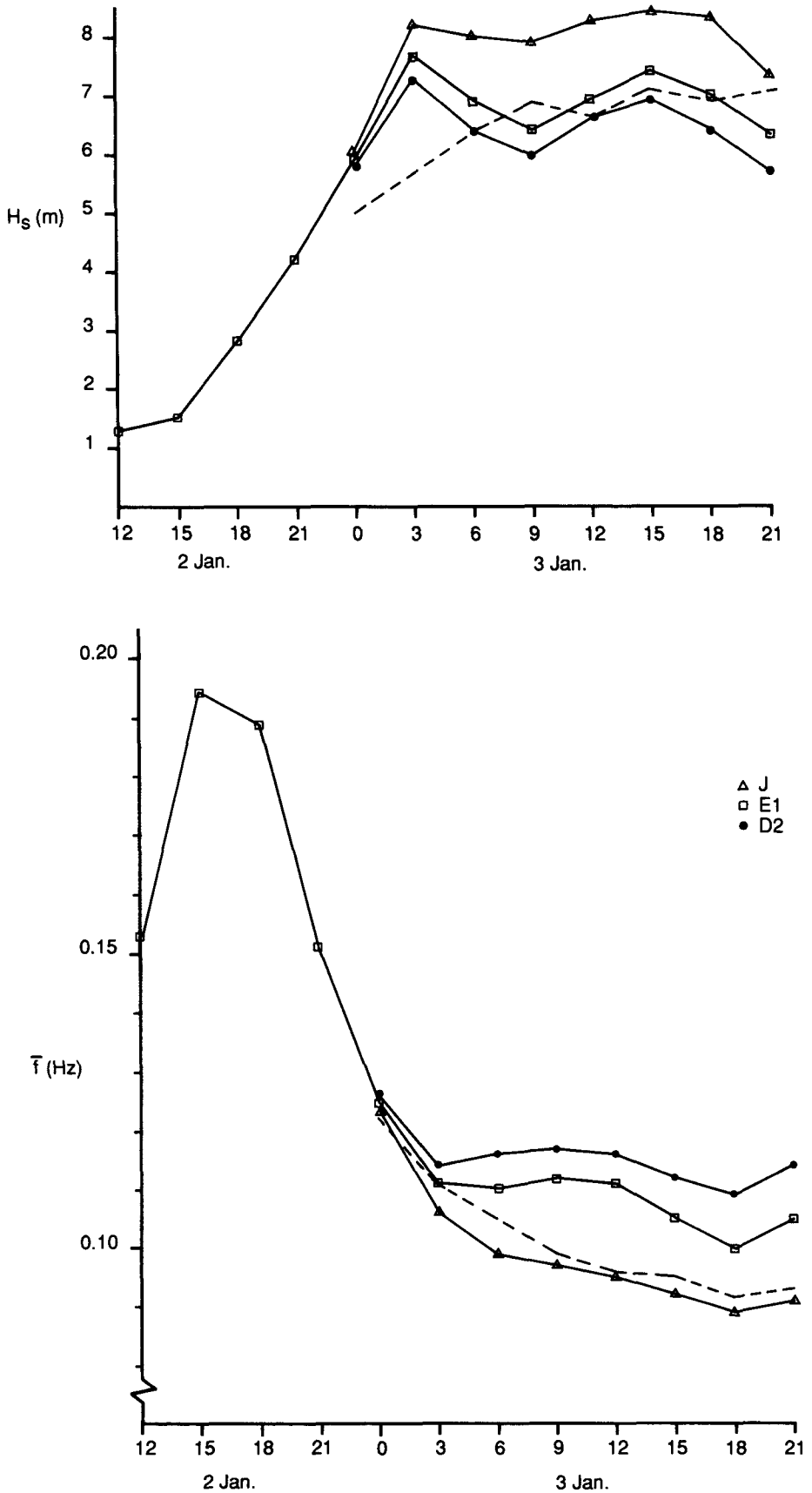

FIG. 5. (a) Significant waveheight H_s at Texel from 1200 UTC 2 January to 2100 UTC 3 January: the eddy-viscosity model (E1), the drag law (D2), the empirical expression (J), and as measured (dashed). (b) Same for the mean frequency $\bar{f}$.

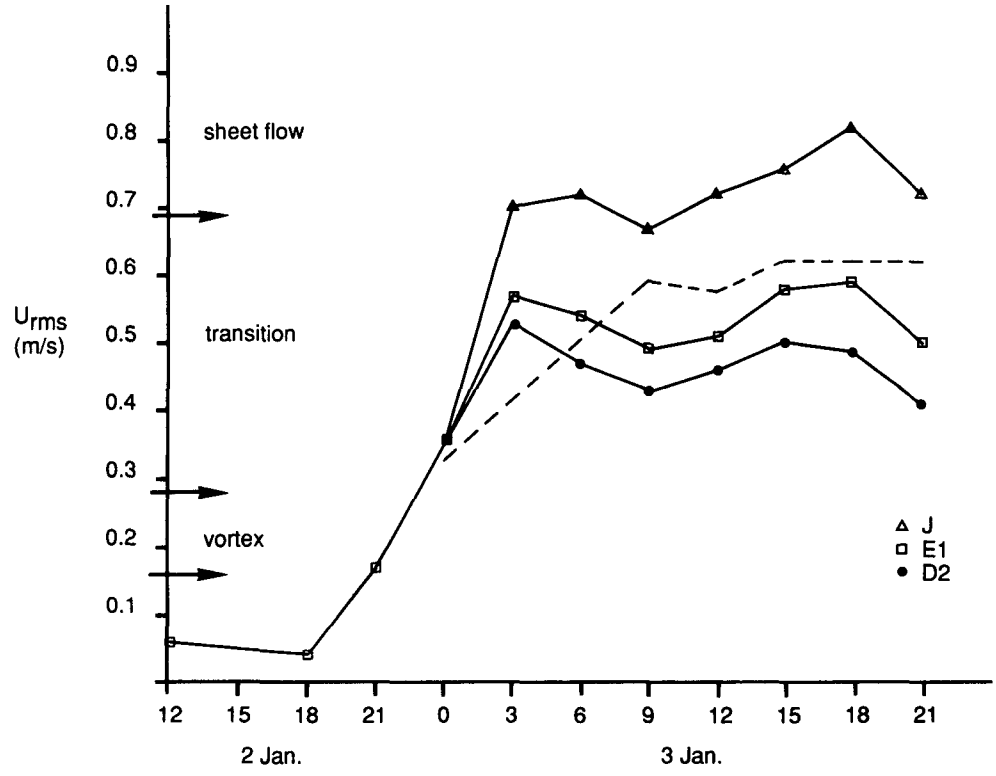

FIG. 6. Same as in Fig. 5 for the root-mean-square bottom velocity U_{rms}. The limits for the different ripple regimes are indicated, see section 8.

served in the early stages of the storm, when the water can be considered as relatively deep. After some time however, the influence of the bottom is felt. This is expressed by the parameter $k_p h$. The nonlinear transfer slightly increases for decreasing $k_p h$ values because of the factor R in (5.4): $R(2) = 0.85$ and $R(1) = 1.25$. This gives an increased transfer of energy from the higher frequencies to the low-frequency part of the wave spectrum for decreasing relative water depths. At the same time, however, the bottom dissipation is felt more strongly on the low-frequency part of the spectrum because of the increase in the factor $k/\sinh 2kh$ in (2.1).

The ratio of bottom dissipation to dissipation by whitecapping is given by

$$\frac{S_{bot}}{S_{dis}} = \frac{\bar{k}}{2.6\bar{\omega}(E\bar{k}^2)^2} \frac{C}{\sinh 2kh}. \qquad (5.5)$$

The only factor in (5.5) that changes appreciably during the storm is the hyperbolic sine. For high frequency waves kh is large and the ratio (5.5) always remains small. For the energy containing range of the spectrum ($k \sim k_p$) one finds for the equilibrium phase of the storm:

$$\frac{S_{bot}}{S_{dis}} \sim 3 \quad \text{for Texel}$$

$$\frac{S_{bot}}{S_{dis}} \sim 2 \quad \text{for Eurochannel.}$$

(For Texel the value given by E1 for C is used, because this is probably the most realistic value.) Bottom dissipation is thus seen to dominate over dissipation by whitecapping at the height of the storm.

Now there is one term left in the energy balance equation (5.1), which has to be evaluated. For lack of more measured data the advection term has to be estimated partly from the model results. (Assuming that the model bias is roughly homogeneous in space, this should be adequate.) The total advection can be estimated as

$$\int_{\mathbf{k}} c_g \nabla F(\mathbf{k}) d\mathbf{k} \sim c_g(f_p) \frac{\Delta E}{\Delta x}$$

where $c_g(f_p)$ is the group velocity, which corresponds to the peak frequency. At Texel the energy gradient is typically 2 m^2 per 100 km and the group velocity $c_g \sim 10$ m s^{-1}. This gives a total advection of the order of magnitude of 10^{-4}, which is comparable to the other

source terms. At Eurochannel advection is less significant, with a typical energy gradient of 0.7 m^2 per 100 km and $c_g \sim 8$ m s^{-1}. This smaller advection rate is explained by the fact that at Eurochannel the fetch consists of shallow water where the advected wave energy is strongly dissipated by bottom friction, while at Texel the fetch is mostly deep water. The strong advection at Texel probably causes the continuing downshift of the peak frequency for low $k_p h$ values, which is not present at Eurochannel. The balance that is attained between S_{nl}, S_{bot}, and advection for the low-frequency part of the wave spectrum eventually stops

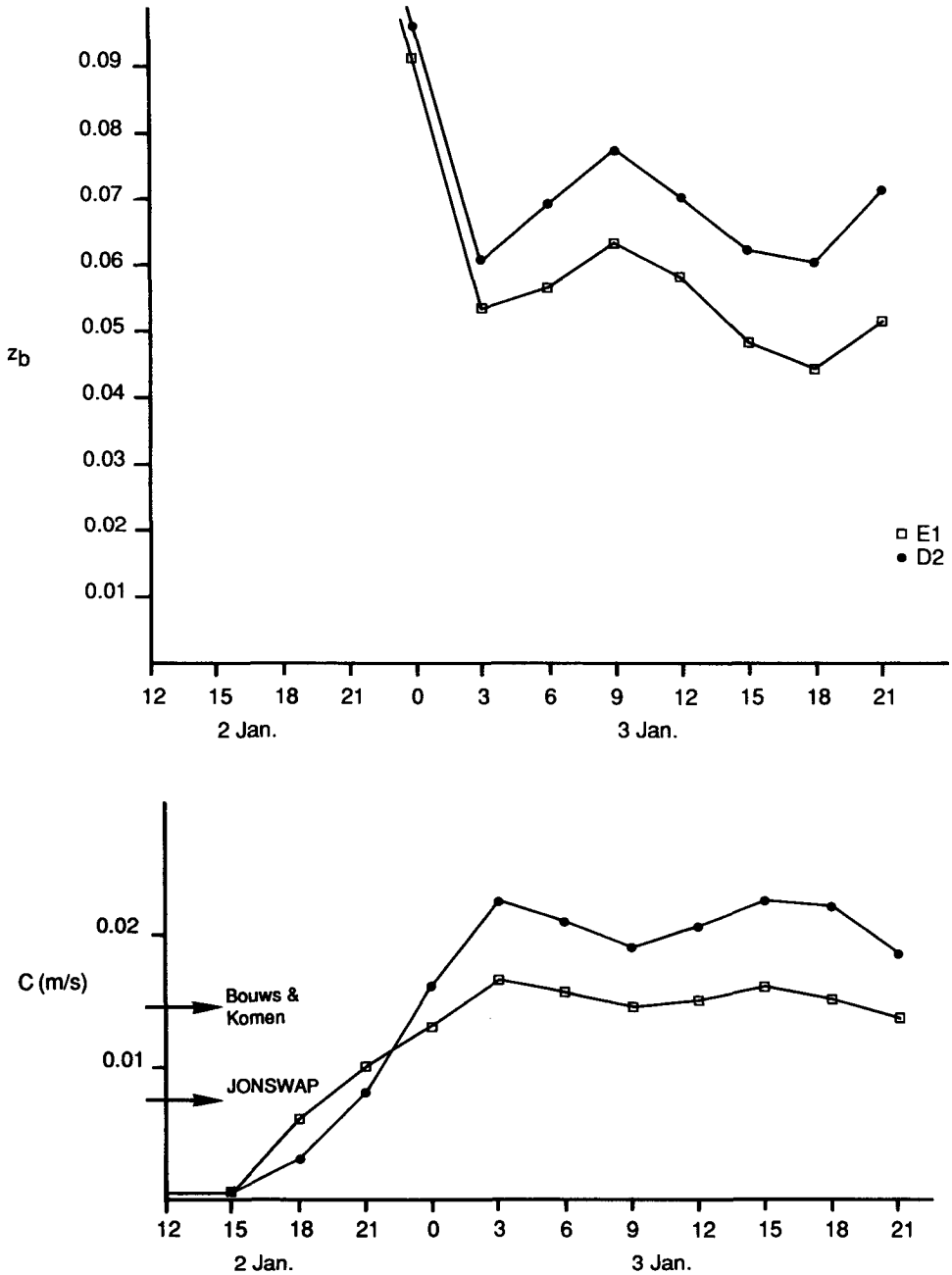

FIG. 7. (a) The dimensionless roughness parameter z_b at Texel from 1200 UTC 2 January to 2100 UTC 3 January: the eddy-viscosity model (E1) and the drag law (D2). (b) Same but for the dissipation coefficient C. The mean JONSWAP value and the value proposed by Bouws and Komen (1983) are indicated.

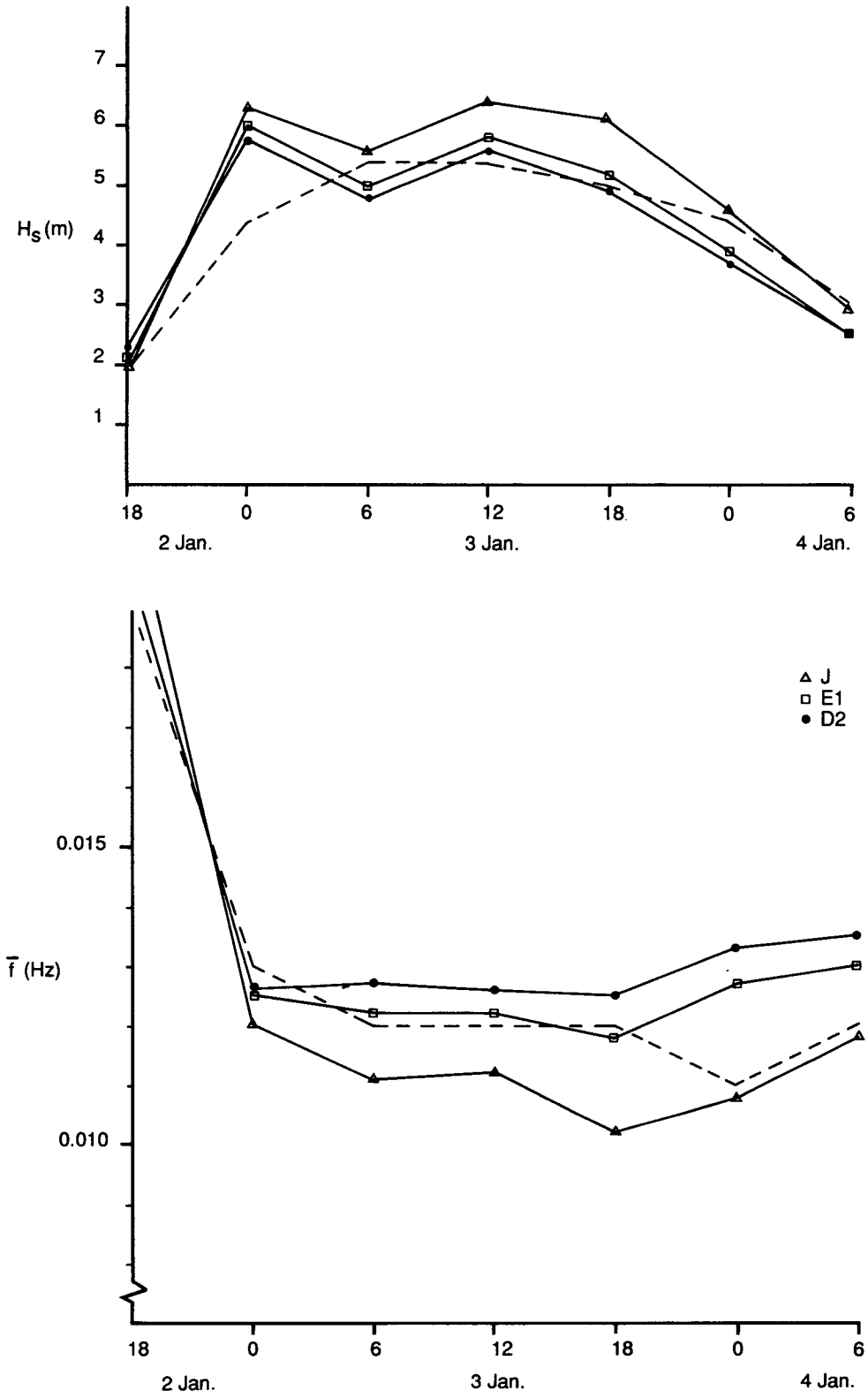

FIG. 8. (a) The significant wave height H_s at Eurochannel from 1800 UTC 2 January to 0600 UTC 4 January: the eddy-viscosity model (E1), the drag law (D2), the empirical expression (J), and as measured (dashed). (b) Same for the mean frequency $\bar{f}$.

TABLE 1. Parameters in the energy-balance equation for Texel and for Eurochannel.

	Texel midnight	Texel equilibrium	Eurochannel equilibrium
$u_a^*/c_p(f_p)$	0.09	0.08	0.08
$E\bar{k}^2$	0.006	0.005	0.005
$k_p h$	1.6	1.1	1.4
C [E1 (m s^{-1})	0.013	0.016	0.015
C [D2 (m s^{-1})	0.014	0.025	0.015
c_g (m s^{-1})	8	12	8
$\bar{\omega}/\bar{k}$ (m s^{-1})	12	14	12

the down shifting of the peak frequency. For shallow water the additional dissipation source term creates an equilibrium before the wind input in the energy containing range of the wave spectrum stops (see also Weber 1988). This point is reached for Eurochannel at 0600 and for Texel at 1200.

All three hindcasts show an overprediction of H_s at the beginning of the storm. The integral wave steepness $E\bar{k}^2$ is increased by about a factor of two by this overprediction in H_s. This results in an increased dissipation by whitecapping and, therefore, in a reduced wave growth. At the same time the peak frequency goes down because of the increased transfer rate to the lower wave frequencies. In E1 and D2 the bottom dissipation is also enhanced as the dissipation coefficient depends on the (increased) bottom velocity. An enhanced bottom dissipation counterbalances the added energy input to the lower frequencies by the nonlinear transfer in E1 and in D2. The steepness parameter is thus reduced in J by a decrease both in H_s and in $\bar{f}$, while in E1 and in D2 the decrease in H_s is more pronounced and $\bar{f}$ remains at a higher level.

The advected low-frequency wave components are strongly affected by the enhanced bottom dissipation in E1 and in D2. This contributes at least partly to the high mean frequency values. The overprediction in the mean frequency in E1 and in D2 causes a decrease in the bottom dissipation. This holds especially for D2, where C is proportional to the (decreased) bottom velocity. There is, however, also a decrease in the advection rate and in the nonlinear energy transfer.

The balance between the various source terms in (5.1) is delicate and complicated. A qualitative analysis of the model response to an error in one of the parameters is therefore necessarily speculative. A quantitative investigation would be instructive, but is outside the scope of this paper.

Summarizing the foregoing: the hindcast results are not conclusive with regards to $\bar{f}$. The strong advection rate at Texel explains the coutinuing down shift of the mean frequency, while at Eurochannel the equilibrium is attained much earlier. At Eurochannel E1 gives the best results for the mean frequency, but at Texel E1 yields values that are too high. It is not clear whether the eddy-viscosity dissipation coefficient is simply too high here or whether the chain of reactions that follows the overprediction in the significant wave height causes the high mean frequency value. In view of the superior prediction of the significant wave height, the eddy-viscosity model is nevertheless to be preferred to the empirical expression.

6. The swell hindcast

An intense storm took place in the Norwegian Sea on 13 January 1980, generating swell that propagated in a south-southeast direction. Low-frequency waves started to arrive at the Dutch coast on 15 January. This case of swell is characterized by relatively high wave heights (1–2 m) and long periods. The peak frequency is 0.06 Hz and the energy-containing range of the swell spectrum extends from 0.05 to 0.12 Hz. Wind conditions were very mild in the southern North Sea during that time. The balance is now between bottom dissipation and advection. The wave steepness is so low ($E\bar{k}^2 \sim 10^{-5}$) that S_{dis} and S_{nl} are negligible.

Again hindcasts were made with different expressions for the dissipation coefficient C in S_{bot}: the mean JONSWAP value (J), the approximate eddy-viscosity expression (E1), and the drag-law expression (D2). For swell the mean JONSWAP value usually gives accurate results. The input wind field is based on the standard KNMI numerical weather analysis. Hindcast results are compared with six-hourly measurements from Eurochannel.

In Fig. 9a,b predicted values for H_s and H_{s10} are shown for Eurochannel; H_{s10} is used to characterize the energy content of the low-frequency part of the wave field and is defined by

$$\frac{H_{s10}^2}{16} = E_{10} = \int_0^{0.1} F(f)df.$$

There is little difference in predicted values from the three hindcasts. The arrival time of the swell (0600 UTC 15 January) is well predicted, which indicates good accuracy for the peak frequency. This is indeed the case, as all three hindcasts reproduce the measured value within 0.003 Hz. Hindcast results for H_{s10} are very close to the measured values except at arrival time, when there is an overprediction by 50 cm.

The rms bottom velocity and the dissipation coefficient are depicted in Figs. 10a,b. The nondimensional bottom roughness $z_b \sim 0.15$ from the arrival time onwards, so that C_{eddy} and C_{drag} are equal (see Fig. 2). They lie slightly below the mean JONSWAP value. The eddy-viscosity model yields $u^* \sim 2$ cm s^{-1} and the boundary layer thickness is 30 cm. The directional spread $A \sim 0.98$ (nearly one-dimensional) and the main axis of the bottom stress coincide with the direction of propagation within 5° both in E1 and in D2.

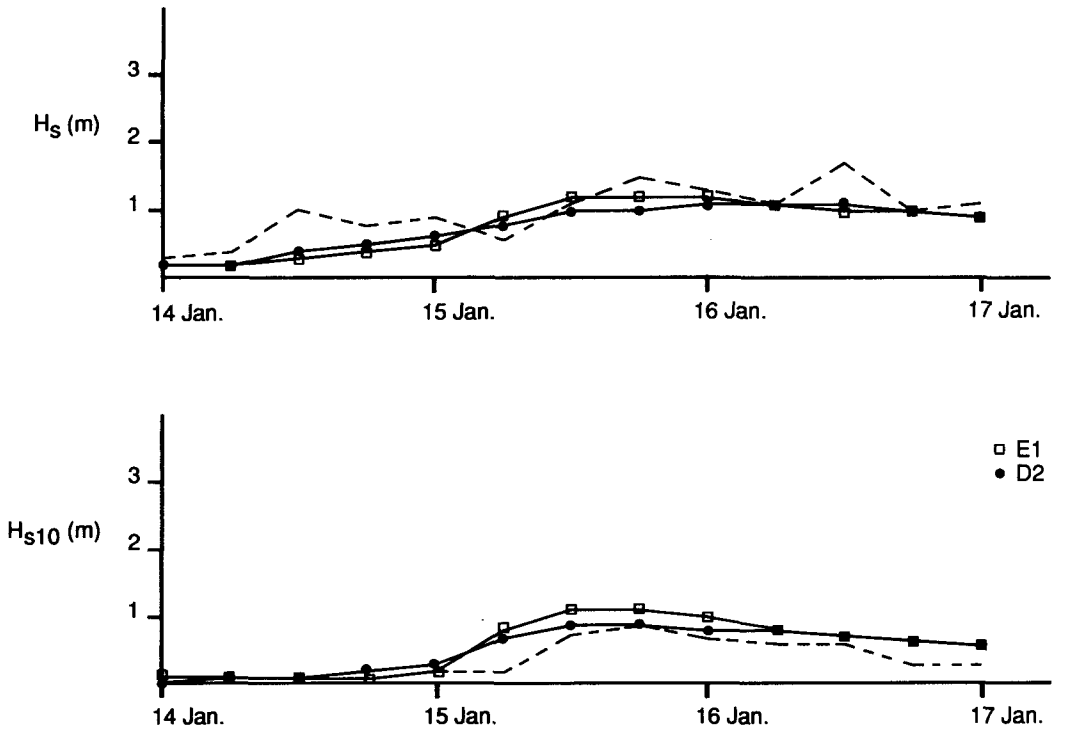

FIG. 9. (a) The significant wave height H_s at Eurochannel on 14–17 January 1980: the eddy-viscosity model (E1), the drag law (D2), and as measured (dashed). (b) Same for H_{s10}.

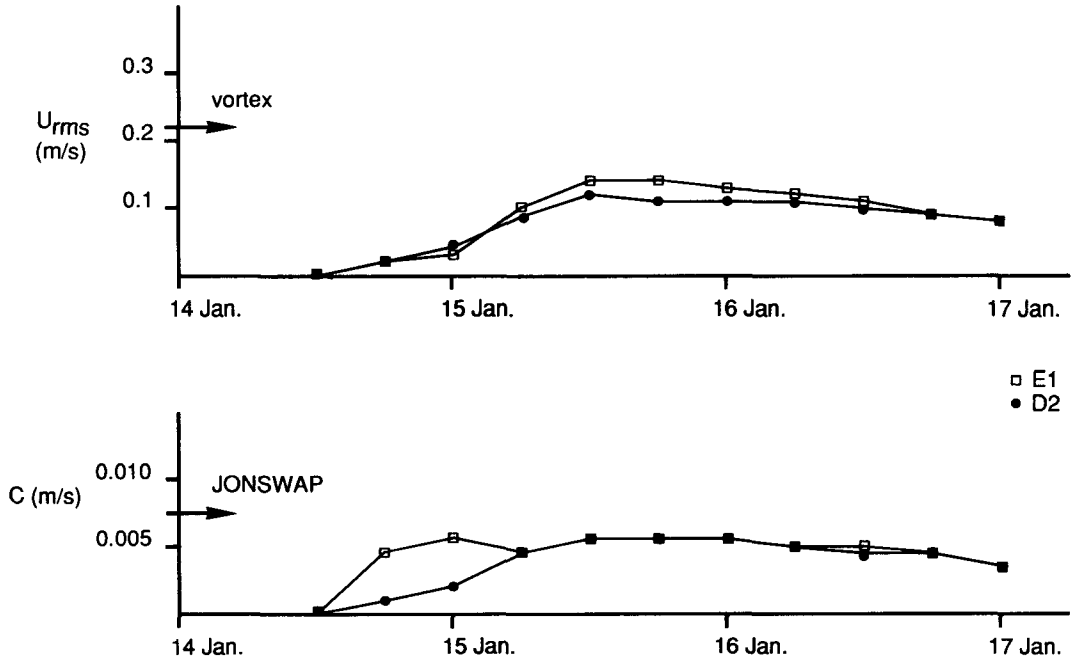

FIG. 10. (a) The root-mean-square bottom velocity U_{rms} at Eurochannel on 14–17 January 1980: the eddy-viscosity model (E1) and the drag law (D2). The limit for ripple formation is indicated, see section 8. (b) The dissipation coefficient C. The mean JONSWAP value is indicated.

7. The tidal current

In the preceding sections the tidal current has been neglected. In a combined wave–current situation this is not necessarily justified and an estimate of the error involved is needed.

In the region off the Dutch coast the tidal current is semidiurnal and rotates 360° clockwise over the tidal cycle. The major axis is roughly parallel to the coast (direction north-northeast to south-southwest) with peak flows up to 0.6 m s^{-1}. The tide turns quickly over the transverse direction, in the coastal region with strongly reduced current speeds. At Texel and Eurochannel the current is virtually parallel to the coast. The variation in water depth due to the tide is 1.5 m. At low tide the factor $k/\sinh 2kh$ in S_{bot} is therefore increased by 10% at most, and at high tide this factor is decreased also by 10% at most. This effect is not taken into account.

Current refraction can be neglected in the present situation because the group velocity of the energy-carrying waves is of the order of 10 m s^{-1}, which is one order of magnitude greater than the current velocity. Also the Doppler shift of the wave frequency is negligible.

The interaction of the wave motion and the tidal current in the vicinity of the bottom is possibly of more importance. Models for the combined (monochromatic) wave–current interaction have been developed by Grant and Madsen (1979) and by Christoffersen and Jonsson (1985). Both models are based on a two-layer eddy-viscosity assumption. The eddy viscosity in the current boundary layer scales with a friction velocity, derived from the mean bed shear stress. In the wave boundary layer the eddy viscosity is related to a friction velocity, based on the maximum bed shear stress. Both the mean and the oscillatory motion therefore contribute to the friction velocity in the wave boundary layer. The model of Christoffersen and Jonsson (henceforth denoted as CJ) is somewhat easier to apply than the Grant and Madsen model. Therefore I will use CJ to estimate the mutual influence of the waves and the tide.

In a combined monochromatic wave–current situation the wave energy dissipation and the current energy dissipation are determined iteratively in CJ, starting from the uncoupled wave and current dissipation. The parameters, which define the iteration, are

$$\left.\begin{aligned} p_1 &= \frac{k_N \omega}{U_{max}}; \quad p_2 = \frac{h}{k_N}; \\ p_3 &= \frac{U_{cur}}{U_{max}}; \quad p_4 = \theta_{cur} - \theta \end{aligned}\right\}. \qquad (7.1)$$

Here U_{max} is the maximum bottom orbital velocity, U_{cur} is the depth-averaged mean current and $\theta_{cur} - \theta$ is the angle between the current and the wave motion. For monochromatic flows $U_{max} = \{2\langle U^2\rangle^{1/2}\}$ (here $\langle\cdot\rangle$ denotes the period mean). In a pure wave situation the wave energy dissipation is determined by p_1 and the wave bottom velocity. For a current alone the dissipation is determined by p_2 and the current velocity. The wave–current interaction mainly depends on p_3, but is stronger for a codirectional current than for a current perpendicular to the waves.

TABLE 2. Parameters in CJ for Texel and for Eurochannel.

	Texel storm		Swell
	Texel	Eurochannel	Eurochannel
p_1	0.04	0.06	0.1
p_2	750	625	625
p_3	0.75	1	3
p_4	0°	0°	90°

The approximate eddy-viscosity model, derived in section 3, has a similar structure to the monochromatic eddy-viscosity model; U_b and ω_p correspond to U_{max} and ω. (The eddy-viscosity model presented in this paper differs from CJ in the pure wave limit, because the friction velocity is defined in terms of an ensemble mean value instead of a maximum value as in CJ. This yields slightly different results.) It seems reasonable to assume that CJ can be extended to the random wave case, replacing monochromatic quantities by the analogous random quantities. This means that the radian peak frequency is used and that U_{max} is replaced by $2^{1/2}\langle U^2\rangle^{1/2}$ in (7.1). It follows that p_1 is proportional to z_b.

The strength of the interaction can now be estimated from CJ, using $U_{cur} = 0.6$ m s^{-1}. The parameters p_1–p_4 are given for Texel and for Eurochannel in Table 2. For the wind sea $p_4 = 0°$ has been used to obtain an upper limit. It was found that the presence of the current increases the wave dissipation by less than 5% at both stations. The wave motion gives rise to an apparent bottom roughness of 35 cm (Texel) and 25 cm (Eurochannel), which replaces the physical roughness value in (7.1). The current energy dissipation is increased by 60%–70%. One is clearly justified in neglecting the current and the Texel storm can be regarded as a typical wave-dominated situation.

For the swell, the modification of the wave dissipation due to the current is less than 10%, which is just acceptable. The current dissipation increases by about 30%, with an apparent bottom roughness of 12 cm. For less extreme swell (lower amplitudes and shorter periods) the tidal signal is indeed visible and the influence of the current is not negligible.

Bottom friction is important either if U_{rms} is large (wind sea) or if the frequencies are low (swell). The foregoing indicates that for a range of situations, where one of these conditions hold, the influence of the tide on the wave dissipation is small. This agrees with JONSWAP, where no dependence of the dissipation coef-

ficient on the tidal phase or velocity was found. It seems, however, to contradict the analysis of the wave–current interaction given in JONSWAP, which was based on Hasselmann and Collins (1968).

The basic difference between CJ and Hasselmann and Collins is that the latter treat the combined wave–current flow in a one-layer model, where the total bottom stress is related to the total velocity field through the quadratic drag law (4.1). Adding the tidal velocity to the wave bottom velocity thus results in a strong increase in the bottom stress. The drag coefficient is assumed to be constant and the possible modification of the drag coefficient due to the tidal current is not taken into account. The drag coefficient for the wave field is of the order 10^{-2}, as was seen previously. This is one order of magnitude larger than the drag coefficient for the tidal current (Sternberg 1968). Intuitively one would therefore expect that the total stress cannot be related to the added wave and current velocity in a drag-law formulation. A two-layer eddy-viscosity model like CJ seems to give a much more realistic description of the wave–current interaction than a one-layer drag law.

8. The roughness value

Presumably the roughness value $k_N = 4$ cm reflects the presence of sand ripples of a few centimeters height on the sea bed. In a combined wave–current flow field these can be generated either by the waves or the current or both. Recently Amos et al. (1988) have measured the threshold values for sand traction and bedform generation for fine sand ($D_m = 0.23$ mm) in 22 m of water on the Canadian continental shelf. The peak tidal current near the measuring site was 45 cm s^{-1} and during the measuring period the rms bottom orbital velocities ranged from 8 to 30 cm s^{-1}, with frequencies around 0.12 Hz. These conditions are comparable to the southern North Sea wave–current climate.

Amos et al. found that for high wave activity the pure wave threshold criterion holds. For low wave activity, however, the threshold is influenced by the superimposed mean flow such that the threshold can be reduced by as much as a factor of two for increasing mean currents. The pure current threshold criterion applies for extreme low wave activity. Ripples were seen over a wide range of flow conditions.

The consistency of the roughness value $k_N = 4$ cm with the flow and sediment conditions will now be checked. The amount of motion of the bottom material is determined by the ratio of the bottom shear stress to the restoring force of gravity. This ratio is called the Shields relative stress parameter (see e.g., Sleath 1984):

$$\theta_S = \frac{\tau_{\max}(y_0)}{(\rho_s - \rho)gD_m} \tag{8.1}$$

where ρ_s is the sediment density. The sediment grain size is taken as $D_m = 0.25$ mm and quartz density $\rho_s = 2.65 \times 10^3$ kg m^{-3} can be assumed for the sand. The value of the stress has to be estimated from the bottom orbital velocity and the scaled bottom roughness using a parameterization. The influence of the tidal current on the bottom stress was seen to be small for the cases considered here. For the onset of grain motion θ_S, and thus $\tau_{\max}(y_0)$, has to exceed a critical value. This value is reached for a lower orbital velocity if the sea bed is rippled or if it is roughened by bioturbation than for a flat bed, as the roughness value is enhanced for a rippled or roughened bed. Empirical relations for ripple formation and ripple geometry have been given by a number of authors, see Sleath (1984) for an overview.

For the storm and swell cases considered here, the scaled roughness z_b varies by a factor two for a flat bottom; this results in a variation of 10% in u^*/U_b (see Fig. 1). This is negligible, given the uncertainty in the empirical relations for ripple formation and in our knowledge of the actual situation. Therefore the stress can be replaced in the Shields parameter by the (known) velocity at the bottom. This yields

$$\tilde{\theta}_S = \frac{\rho U_{\max}^2}{(\rho_s - \rho)gD_m}. \tag{8.2}$$

This form is used by Dingler and Inman (1976), who obtain $U_{\max}$ for the random wave field from the wave height, the peak frequency, and the water depth. Replacing $U_{\max}^2$ by $2\langle U^2 \rangle$ yields closely the same results.

Dingler and Inman distinguish different ripple regimes, depending on the value of $\tilde{\theta}_s$. The bed is planar for $\tilde{\theta}_s < \tilde{\theta}_t$, where $\tilde{\theta}_t$ is the threshold value for the onset of grain motion. This value is given as $\tilde{\theta}_t \sim 1.7/f$, with f the wave frequency. At increasing wave intensity, with $\tilde{\theta}_t < \tilde{\theta}_S < 40$, vortex ripples form. These are characterized by a constant ripple steepness value of 0.15. The transition from this regime to sheet flow occurs in the range $40 < \tilde{\theta}_S < 240$. The ripple steepness then decreases from 0.15 to 0.05 as the ripple height decreases, while the ripple length remains constant. For $\tilde{\theta}_S > 240$, several layers of sand move in sheet flow. These criteria were derived both from laboratory and field data for a wide range of ripple regimes. It was found that under intense wave motion the ripple regime is established within a few wave cycles.

The prevailing ripple regime during the Texel storm can now be estimated from (8.2) by applying the limits given above. Both at Texel and at Eurochannel the threshold value can be taken as $\tilde{\theta}_t \sim 16$, using $f \sim 0.12$ Hz. It is then found that at Texel the bottom orbital velocity passes rapidly through the vortex ripple regime by 2100 UTC 2 January and remains in the transition regime during the entire storm (see Fig. 6). At Eurochannel the bottom velocity is estimated from the eddy-viscosity hindcast, which is closest to the measured values. During the equilibrium phase of the storm $U_{\text{rms}} \sim 45$ cm s^{-1}, which is also in the transition regime. The ripple steepness can be estimated as 0.05–0.08,

with a ripple length of 20–40 cm (Dingler and Inman 1976), so that the ripple height ranges 1–3 cm. The roughness value used is thus applicable during the period that the water can be considered as shallow and bottom friction is important.

For swell the threshold value for the onset of sand motion is larger than for the wind sea during the Texel storm, as this value is inversely proportional to the wave frequency. For $f = 0.06$ Hz, the threshold stress $\tilde{\theta}_t = 28$, well above the value of the Shields relative stress parameter for Eurochannel ($\tilde{\theta}_S \sim 7$); see also Fig. 10. Now the roughness value cannot be explained from the waves alone (apart from relict ripples). The current velocity is, however, above the pure current threshold value, so that it is likely that current-induced sand ripples are present. The geometry of these ripples is different from the geometry of wave-induced ripples and no attempt will be made to estimate k_N from the tidal current. The roughness value has been determined experimentally in a pure current situation for a range of bed types (rippled sand, gravel, rocks) by Sternberg (1968). He found that the roughness length ranges from 0.6–6 cm in the hydrodynamically rough regime, which includes the value used in the present study.

The roughness value of 4 cm is thus seen to be acceptable both for the storm and for the swell case. It should be kept in mind that the time and length scales of the wave model are orders of magnitude larger than the time and length scales of the roughness elements. The roughness value used should therefore be regarded as an average value over a model gridbox and an integration timestep. There is no pretention that this value is realistic at every moment and place. As the bottom dissipation does not depend sensitively on k_N, the value used need not even be very accurate.

A model to describe the sediment motion dynamically as a function of the fluid flow and the bed material has been developed by Grant and Madsen (1982). Implementation of this process in a wave model results in a dependence of the wave parameters on the sand grain diameter (Tolman 1990), which is clearly not realistic. For large scale models the use of a fixed roughness length seems to be preferable to dynamically modeling the sediment–wave–current interaction. For fine scale models of near-coastal areas and estuaries this approach might however be inadequate.

9. Summary and conclusions

An empirical expression for the spectral energy dissipation due to friction in the turbulent bottom boundary layer is

$$S_{\text{bot}} = -C \frac{k}{\sinh 2kh} F(\mathbf{k}) \qquad (2.1)$$

where C is a dissipation coefficient with the dimension of a velocity. The mean JONSWAP value $C = 0.0077$ m s^{-1} generally gives good results for swell in the southern North Sea. For wind sea during storm conditions this value is much too low. Assuming a certain parameterization of the turbulent stress in the bottom boundary layer, C can be determined in terms of the wave field and the bottom conditions. Two parameterizations were considered: the eddy-viscosity model and the quadratic drag law.

In the eddy-viscosity model the bottom boundary layer can be characterized by one dimensionless variable z_b, if it is assumed that the bottom velocity spectrum is narrow and single peaked. This variable is a function of the ratio between the bottom roughness length and the boundary layer thickness. The coefficient C_{eddy} can be expressed in terms of z_b and a velocity U_b (which represents the free stream orbital velocity at the top of the boundary layer) as

$$\tilde{C}_{\text{eddy}} = \exp(-8.34 + 6.34 z_b^{0.08}) U_b. \qquad (3.15)$$

The eddy-viscosity dissipation coefficient depends explicitly on the bottom roughness length k_N, which again depends on the fluid flow and on the sediment. A roughness value, which corresponds to the sand grain diameter, was found to yield a dissipation rate that is much too low to be realistic. Therefore, it was assumed that sand ripples are present, and as a first guess a constant roughness value of 4 cm was used. For wind sea during a storm this roughness value can be associated with wave-induced sand ripples, as the near-bottom orbital velocities are large enough to initiate sand motion. For swell this is not the case and the roughness value should be associated with current ripples or with relict ripples. The use of a constant roughness value can be regarded as a subgrid parameterization of the dynamics of the sediment–wave–current interaction, comparable to the use of a representative roughness length for large areas in atmospheric models.

The application of the eddy-viscosity model is restricted to cases where (i) the boundary layer is turbulent and (ii) no sheet flow occurs. The first condition implies that the near-bottom orbital velocity should not be too low (5–10 cm s^{-1}), while the second condition imposes an upper limit on the velocity (70 cm s^{-1} for fine sand). Bottom friction, as described by the eddy-viscosity model, can only be significant if these conditions are fulfilled.

Assuming a drag-law parameterization Hasselmann and Collins (1968) determined an expression for the bottom dissipation, which has the form (2.1), with C given by

$$C_{\text{drag}} = -2 c_D \langle U_1^2 \rangle^{1/2} \{ F_1(A) \cos^2(\theta - \phi) + F_2(A) \sin^2(\theta - \phi) \}. \qquad (4.2)$$

Here $\langle U_1^2 \rangle^{1/2}$ and the directional spread A follow from the bottom orbital velocity spectrum. The angle $\theta - \phi$ represents the direction of a wave component relative to the main axis of the bottom velocity spectrum and c_D is a drag coefficient. Hasselmann and Collins pro-

posed a constant value $c_D = 0.015$; the dissipation coefficient then only depends on the bottom velocity. Naturally the same limits apply for the bottom velocity as in case of the eddy-viscosity model.

The eddy-viscosity model (E1) and the drag law (D2) were tested in a hindcast of a severe depth-limited storm with a regional version of the third-generation WAM model. In the standard version of WAM the bottom dissipation is given by the empirical expression (2.1), with the mean JONSWAP value $C = 0.0077$ m s^{-1} for the dissipation coefficient (J). For the Texel storm E1 yields a dissipation coefficient $C = 0.015$ m s^{-1} and D2 gives a value $C = 0.019$ m s^{-1}. The stronger bottom dissipation in E1 and D2 causes a reduction in the significant wave height and an increase in the mean frequency compared to the results using J. The predicted values for the significant wave height were found to be much improved in E1 and in D2. At one station the mean frequency is best predicted by J, while at the other station E1 gives the best results.

The value for the dissipation coefficient found in E1 is closest to the value proposed by Bouws and Komen (1983) for this storm. The coefficient found in D2 is too high and the mean JONSWAP value is too low. This means that the equilibrium situation, where both H_s and $\bar{f}$ remain constant, is best simulated using the eddy-viscosity expression for S_{bot}.

A hindcast was also made for a case of swell with extremely high amplitude and low frequency. Here both E1 and D2 closely reproduce the mean JONSWAP value for the dissipation coefficient. All three hindcasts predict the significant wave height and the arrival time accurately.

In the present study the influence of the tide was estimated applying the combined wave–current eddy-viscosity model of Christoffersen and Jonsson (1985) to the random wave case. It was found that for a range of wave conditions, common to the southern North Sea, the influence of the tidal current on the wave dissipation due to bottom friction is small. This is supported by the fact that the tidal signal is indeed not seen in the measurements both for the storm and for the swell.

The eddy-viscosity model thus qualitatively agrees with the JONSWAP results for swell attenuation: the dissipation coefficient does not depend on the tidal phase or velocity and there is a negligible dependence on the wave frequency. For wind sea there should however be a dependence on the wind (friction) velocity (see Fig. 3). For a more detailed comparison the JONSWAP cases would have to be classified according to the limits of applicability given earlier for the eddy-viscosity model. Other mechanisms than bottom friction should be used to explain the observed wave attenuation for the cases with low near-bottom orbital velocities.

Both E1 and D2 show a partial improvement compared to J in the Texel storm hindcast, although the hindcast results are not as conclusive as one would like them to be. E1 performs slightly better than D2. For swell E1 and D2 reduce to J, which generally gives good results. The eddy-viscosity model has an advantage over the drag law in that it can be extended to the combined random wave–current situation. This predicts a negligible influence of the tide on the wave energy dissipation, in agreement with the measurements. The explicit dependence of E1 on the roughness length seems to be a drawback. The dissipation rate is however not sensitively dependent on the roughness length, while a constant value $k_N = 4$ cm is found to be adequate for the range of conditions considered here. It seems worthwhile to perform more extensive tests with E1 both for idealized situations and for real storm events. The eddy-viscosity model is considered to be a promising alternative to the empirical expression used now in the WAM model.

Acknowledgments. Various members of the WAM group contributed to this research by their interest and criticism. I would like to thank one referee for his comment on sand motion. Financial support was provided by the research community Meteorology and Physical Oceanography (MFO) of the Netherlands Organisation for Scientific Research (NWO).

APPENDIX A

A Spectral Eddy-Viscosity Model

In this appendix an outline of the eddy viscosity model is given. A more extensive account can be found in Weber (1989).

The momentum equation for the boundary layer flow can be derived by elementary scale analysis of the Navier–Stokes equations (Schlichting 1955) as

$$\frac{\partial}{\partial t}(\mathbf{u} - \mathbf{U}) = \frac{1}{\rho}\frac{\partial}{\partial y}\tau. \tag{A1}$$

Here $\mathbf{u} = (u_1, u_2)$ is the horizontal velocity in the bottom boundary layer, which can be written as a sum of velocity components analogous to (2.2) and (3.2). In the eddy-viscosity model the stress is parameterized as ($i = 1, 2$)

$$\frac{\tau_i}{\rho} = \kappa u^* y \frac{\partial u_i}{\partial y}. \tag{A2}$$

The boundary conditions are

$$\mathbf{u} = 0 \quad \text{at} \quad y = y_0$$
$$\mathbf{u} \to \mathbf{U} \quad \text{for} \quad y \to 0. \tag{A3}$$

Equations (A1) and (A2) can be solved with the boundary conditions (A3). The turbulent bottom stress is then found as given in (3.2) with

$$T_{\mathbf{k}}(\xi_0) = -\frac{1}{2}\kappa\xi_0 \frac{\text{Ker}'(\xi_0) + i\text{Kei}'(\xi_0)}{\text{Ker}(\xi_0) + i\text{Kei}(\xi_0)}. \tag{A4}$$

Here Ker + iKei is the zero order Kelvin function (Abramowitz and Stegun 1964); the prime denotes the derivative with respect to the argument, given by

$$\xi_0 = \left(\frac{4(y_0 + h)\omega}{\kappa u^*}\right)^{1/2}. \tag{A5}$$

The definition (3.1) of the average friction velocity u^* can be worked out, using the Gaussian distribution function of $\tau(y_0)$. This yields

$$u^* = \sigma_{11}^{1/2} F_3(A) \tag{A6}$$

with $F_3(A) = \Gamma(5/4)^2 2^{1/2} F(-1/4, 1/2, 1, A)^2$, where F is a hypergeometric function with argument $A = 1 - \sigma_{22}/\sigma_{11}$ (Abramowitz and Stegun, Ch. 15, 1964). Equation (A6) holds in a coordinate system that has $\sigma_{12} = 0$ and $\sigma_{22} \leqslant \sigma_{11}$. This coordinate system can be found from the given coordinate system by rotation through an angle ϕ, defined by

$$\phi = \frac{1}{2}\arctan[2\tilde{\sigma}_{12}/(\tilde{\sigma}_{11} - \tilde{\sigma}_{22})]. \tag{A7}$$

(The tildas denote values with respect to the original coordinate system.)

The spectral energy dissipation is given by

$$\frac{\partial}{\partial t} F = -\langle \tau(y_0) \cdot \mathbf{U}_k \rangle. \tag{A8}$$

Substitution of (3.2) with (A4) in (A8) leads to (2.1) with (3.7).

Given a surface elevation spectrum $F(\mathbf{k})$, a water depth h, and a bottom roughness k_N, u^* can be determined as follows:

(i) take an arbitrary initial value u_0^*,
(ii) determine $\tilde{\sigma}_{11}$, $\tilde{\sigma}_{22}$ and $\tilde{\sigma}_{12}$ from (3.6).,
(iii) determine the angle ϕ from (A7),
(iv) perform the rotation through ϕ:

$$\begin{aligned}
\sigma_{11} &= \tilde{\sigma}_{11}\cos^2\phi + 2\tilde{\sigma}_{12}\cos\phi\sin\phi + \tilde{\sigma}_{22}\sin^2\phi \\
\sigma_{22} &= \tilde{\sigma}_{11}\sin^2\phi - 2\tilde{\sigma}_{12}\cos\phi\sin\phi + \tilde{\sigma}_{22}\cos^2\phi \\
\sigma_{12} &= 0,
\end{aligned} \tag{A9}$$

(v) determine the next approximation u_1^* from (A6) using (A9),
(vi) if $|u_1^* - u_0^*| >$ precision then $u_0^* = u_1^*$; return to (ii) else $u^* = u_1^*$; stop.

To determine u^* with a precision of 1% usually requires less than ten iterations.

APPENDIX B

The Bottom Velocity U_b and the Roughness δ_b as Functions of Intergral Spectral Parameters

The characteristic velocity $U_b = \langle U_1^2 \rangle^{1/2} F_3(A)$ can be determined numerically in terms of H_s, ω_p, and $k_p h$ for a given spectrum $F(f)$. In this appendix U_b is calculated for a modified JONSWAP spectrum. The eddy-viscosity dissipation coefficient $\tilde{C}_{\text{eddy}}$ is thus found in terms of H_s, ω_p, $k_p h$ and k_N. For an idealized fetch-limited situation, $\tilde{C}_{\text{eddy}}$ can then be related to the fetch, the wind friction velocity, and the water depth by using empirical growth curves for H_s and ω_p.

The modified JONSWAP spectrum is given by

$$F(f) = \frac{\alpha g^2}{(2\pi)^4 f_p f^4} \exp -\left(\frac{f_p}{f}\right)^4 \gamma^\Gamma$$

with

$$\Gamma = \exp\left\{-\frac{(f - f_p)^2}{2\sigma^2 f_p^2}\right\}.$$

Here

$$\sigma = \sigma_a \quad \text{for} \quad f < f_p \quad \text{and} \quad \sigma = \sigma_b \quad \text{for} \quad f \geqslant f_p.$$

This modification was first proposed by Donelan et al. (1985). It results in a f^{-4} dependency for the high frequency range, which was found to give better agreement with measurements. The spectral parameters are $\alpha, f_p, \gamma, \sigma_a$ and σ_b. The standard values $\sigma_a = 0.07$ and $\sigma_b = 0.09$ are used.

The rms bottom velocity U_{rms} and the total energy E can be expressed in terms of the spectral parameters and the nondimensional water depth, if the defining integrals are suitably nondimensionalized. This technique was first used by Kitaigorodskii et al. (1975). It has been applied before by Soulsby (1987) to obtain U_{rms} for various spectral forms. The nondimensional variables used here are

$$\omega_H = \omega\left(\frac{h}{g}\right)^{1/2}, \quad k_H = kh; \tag{B1}$$

ω_H and k_H are related through the nondimensional dispersion relation:

$$\omega_H = (k_H \tanh k_H)^{1/2}. \tag{B2}$$

It now follows that

$$\begin{aligned}
\langle U^2 \rangle &= \frac{\alpha g^2}{f_p}\int_0^\infty \frac{\omega^2}{\omega^4 \sinh^2 kh} \exp -\left(\frac{f_p}{f}\right)^4 \gamma^\Gamma df \\
&= \frac{\alpha g^2}{\omega_{Hp}^3}\int_0^\infty \frac{\omega_{Hp}^2}{\omega_H{}^2 \sinh^2 k_H(\omega_H)} \\
&\qquad \times \exp -\left(\frac{\omega_{Hp}}{\omega_H}\right)^4 \gamma^\Gamma d\omega_H \\
&= \frac{\alpha g h}{\omega_{Hp}^3}\tilde{U}(\omega_{Hp}, \gamma)
\end{aligned} \tag{B3}$$

$$E = \frac{\alpha g^2}{f_p}\int_0^\infty \frac{1}{\omega^4}\exp-\left(\frac{f_p}{f}\right)^4 \gamma^\Gamma df$$
$$= \frac{\alpha h^2}{\omega_{Hp}^5}\int_0^\infty \frac{\omega_{Hp}^4}{\omega_H^4}\exp-\left(\frac{\omega_{Hp}}{\omega_H}\right)^4 \gamma^\Gamma d\omega_H$$
$$= \frac{\alpha h^2}{\omega_{Hp}^5}\tilde{E}(\omega_{Hp}, \gamma). \quad \text{(B4)}$$

A second transformation $\omega_H \rightarrow \omega_H/\omega_{Hp}$ would in fact yield the total energy as $E = \alpha g^2\tilde{E}(\gamma)/\omega_p{}^4$. This transformation is however not meaningful for $\langle U^2\rangle$, because of the hyperbolic sine in $\tilde{U}$. It is therefore not applied to $\tilde{E}$ either.

The integrals $\tilde{U}$ and $\tilde{E}$ can be evaluated numerically. Combining (B3) and (B4) it is found that

$$\frac{\langle U^2\rangle^{1/2}}{E^{1/2}} = \frac{4U_{\text{rms}}}{H_s} = \omega_p Q(k_{Hp}, \gamma) \quad \text{(B5)}$$

with

$$Q(k_{Hp}, \gamma) = (\tilde{U}/\tilde{E})^{1/2}.$$

The factor Q is not sensitive to the value of γ, but varies considerably with k_{Hp}. A good approximation to Q, which can be used for practical purposes, is

$$Q \sim \frac{0.9}{\sinh k_p h}. \quad \text{(B6)}$$

This is accurate up to 5% for $1 \leq \gamma \leq 3.3$ and $0.7 \leq k_p h \leq 2.0$.

The characteristic velocity U_b can be related to U_{rms}, using the definition (3.11) of A:

$$U_b = F_3(A)\langle U_1{}^2\rangle^{1/2} = \frac{F_3(A)}{(2-A)^{1/2}}U_{\text{rms}}. \quad \text{(B7)}$$

For wind sea the spectrum generally has a narrow directional distribution with $A = 0.7$, which gives $U_b = 0.8U_{\text{rms}}$. This will be used in the following. (For near one-dimensional swell, which has $A \sim 1$, it follows that $U_b = 0.7U_{\text{rms}}$.)

Using (B5) and (B7) U_b and z_b can be expressed as

$$U_b = 0.8U_{\text{rms}} = 0.2\omega_p H_s Q(k_p h)$$
$$z_b = \frac{k_N\omega_p}{U_b} = \frac{5k_N}{H_s Q(k_p h)}. \quad \text{(B8)}$$

For idealized situations U_b and z_b can be determined from (B8) in terms of the fetch x, the wind friction velocity u_a^*, and the water depth, using the CERC (1977) growth curves for H_s and ω_p:

$$H_s^* = 160D^* \tanh\{0.0009x^{*0.45}/D^*\}$$
with $D^* = \tanh\{0.0046h^{*0.75}\}$
$$\omega_p^* = 0.03[D_T^* \tanh\{0.016x^{*0.25}/D_T^*\}]^{-1}$$
with $D_T^* = \tanh\{0.077h^{*0.375}\}$ (B9)

All quantities are scaled with the wind friction velocity. The modification u_a^*-scaling was performed by Bouws (Growth curves for wind sea: comparison with the Lake Marken data, unpublished report, in Dutch, 1986).

APPENDIX C

The Drag-Law Model

The expression for the spectral energy dissipation based on the drag-law parameterization (4.1), which is derived by Hasselmann and Collins (1968), is rewritten in this appendix in a form that facilitates comparison with the eddy-viscosity model.

Combining (2.7) and (3.2) in Hasselmann and Collins, S_{bot} is found as $(i, j = 1, 2)$:

$$S_{\text{bot}} = -v_{ij}k_i k_j F(\mathbf{k}) \quad \text{(C1)}$$

with

$$v_{ij} = \frac{gc_D}{\omega^2\cosh^2 kh}\left\{\delta_{ij}\langle U\rangle + \left\langle\frac{U_i U_j}{U}\right\rangle\right\}. \quad \text{(C2)}$$

If the coordinate system is chosen such that

$$\langle U_1 U_2\rangle = 0, \quad \langle U_2{}^2\rangle \leq \langle U_1{}^2\rangle \quad \text{(C3)}$$

then (C2) can be expressed in terms of complete elliptic integrals (Abramowitz and Stegun, Ch. 17, 1964), using the following relations:

$$\langle U\rangle = \left(\frac{2}{\pi}\right)^{1/2}\langle U_1{}^2\rangle^{1/2}E; \quad \left\langle\frac{U_1 U_2}{U}\right\rangle = 0$$
$$\left\langle\frac{U_1{}^2}{U}\right\rangle = \left(\frac{2}{\pi}\right)^{1/2}\langle U_1{}^2\rangle^{1/2}\left[\frac{E}{A} + \frac{A-1}{A}K\right]$$
$$\left\langle\frac{U_2{}^2}{U}\right\rangle = \left(\frac{2}{\pi}\right)^{1/2}\langle U_1{}^2\rangle^{1/2}\frac{1-A}{A}(K-E) \quad \text{(C4)}$$

with $E = E(A)$, $K = K(A)$ the complete elliptic integrals of the first and second kind, respectively, with argument $A = 1 - \langle U_2{}^2\rangle/\langle U_1{}^2\rangle$.

From Abramowitz and Stegun, Chapters 17 and 15, these relations can be rewritten in terms of hypergeometric functions F with argument A (use 17.3.9-10 and Gauss' relations for contiguous hypergeometric functions 15.2.10-27):

$$\left\langle U + \frac{U_1^2}{U} \right\rangle$$

$$= \left(\frac{2}{\pi}\right)^{1/2} \langle U_1^2 \rangle^{1/2} \left\{ \frac{1+A}{A} E + \frac{A-1}{A} K \right\}$$

$$= \frac{1}{2}(2\pi)^{1/2} \langle U_1^2 \rangle^{1/2} \left\{ \frac{1+A}{A} F\left(-\frac{1}{2}, \frac{1}{2}, 1, A\right) + \frac{A-1}{A} F\left(\frac{1}{2}, \frac{1}{2}, 1, A\right) \right\}$$

$$= \langle U_1^2 \rangle^{1/2} F_1(A) \qquad \text{(C5)}$$

with $F_1(A) := \frac{3}{4}(2\pi)^{1/2} F(-1/2, 1/2, 2, A)$

$$\left\langle U + \frac{U_2^2}{U} \right\rangle$$

$$= \left(\frac{2}{\pi}\right)^{1/2} \langle U_1^2 \rangle^{1/2} \left\{ \frac{2A-1}{A} E - \frac{A-1}{A} K \right\}$$

$$= \frac{1}{2}(2\pi)^{1/2} \langle U_1^2 \rangle^{1/2} \left\{ \frac{2A-1}{A} F\left(-\frac{1}{2}, \frac{1}{2}, 2, A\right) - \frac{A-1}{A} F\left(\frac{1}{2}, \frac{1}{2}, 1, A\right) \right\}$$

$$= \langle U_1^2 \rangle^{1/2} F_2(A) \qquad \text{(C6)}$$

with $F_2(A) := \frac{3}{4}(2\pi)^{1/2} F(-1/2, 3/2, 2, A)$.

It now follows that

$$S_{\text{bot}}(\mathbf{k}) = -\{v_{11}k_1^2 + v_{22}k_2^2\} F(\mathbf{k})$$

$$= -2c_D \langle U_1^2 \rangle^{1/2} \{F_1(A) \cos^2(\theta - \phi) + F_2(A) \sin^2(\theta - \phi)\} \frac{k}{\sinh 2kh} F(\mathbf{k}). \qquad \text{(C7)}$$

Here the finite-depth dispersion relation has been used. The angle $\theta - \phi$ represents the direction of a wave component relative to the main axis of the bottom velocity spectrum. This angle appears in (C7) because the wave number (k_1, k_2), as well as the velocity (U_1, U_2), have to be transformed to the coordinate system that has (C3). The direction ϕ of the main axis of the bottom velocity spectrum is defined by:

$$\phi = \frac{1}{2} \arctan[2\langle U_1 U_2 \rangle / \langle U_1^2 - U_2^2 \rangle]. \qquad \text{(C8)}$$

Rotation of the given coordinate system through ϕ yields a coordinate system that has $\langle U_1 U_2 \rangle = 0$. Note that $\langle U_2^2 \rangle \leq \langle U_1^2 \rangle$ can always be achieved by interchanging the role of the x_1 and x_2 axis.

REFERENCES

Abramowitz, M., and I. A. Stegun, 1965: *Handbook of Mathematical Functions.* National Bureau of Standards, Washington, DC.

Amos, C. L., A. J. Bowen, D. A. Huntley and C. F. M. Lewis, 1988: Ripple generation under the combined influence of waves and currents on the Canadian continental shelf. *Contin. Shelf Res.*, **8,** 1129–1153.

Bouws, E., H. Günther, W. Rosenthal and C. L. Vincent, 1985: Similarity of the wind wave spectrum in finite depth water: 1. Spectral form. *J. Geophys. Res.*, **90,** 975–986.

——, and G. J. Komen, 1983: On the balance between growth and dissipation in an extreme depth-limited wind–sea in the southern North Sea. *J. Phys. Oceanogr.*, **13,** 1653–1658.

Cavaleri, L., L. Bertotti and P. Lionello, 1989: A shallow water application of the third-generation WAM model. *J. Geophys. Res.*, **94,** 8111–8124.

CERC (Coastal Engineering Research Center), 1977: *Shore Protection Manual.* Vols. 1–3. Fort Belvoir, Va.

Christoffersen, J. B., and I. G. Jonsson, 1985: Bed friction in a combined current and wave motion. *Ocean Eng.*, **12,** 387–423.

Collins, J. I., 1972: Prediction of shallow-water spectra. *J. Geophys. Res.*, **77,** 2693–2707.

Dingler, J. R., and D. L. Inman, 1976: Wave-formed ripples in nearshore sands. *Proc. 15th Conf. Coastal Engineering,* Honolulu, 2109–2126.

Donelan, M. A., J. Hamilton and W. H. Hui, 1985. Directional spectra of wind-generated waves. *Phil. Trans. Roy. Soc. London,* **A315,** 509–562.

Graber, H. C., and O. S. Madsen, 1988: A finite-depth wind-wave model. Part 1: Model description. *J. Phys. Oceanogr.*, **18,** 1465–1483.

Grant, W. D., and O. S. Madsen, 1979: Combined wave and current interaction with a rough bottom. *J. Geophys. Res.*, **84,** 1797–1808.

——, and O. S. Madsen, 1982: Moveable bed roughness in unsteady oscillatory flow. *J. Geophys. Res.*, **87,** 469–481.

Harding, J., and A. A. Binding, 1978: Windfields during gales in the North Sea and the gales of 3 January 1976. *Meteor. Mag.*, **107,** 164–181.

Hasselmann, K., and J. I. Collins, 1968: Spectral dissipation of finite depth gravity waves due to turbulent bottom friction. *J. Mar. Res.*, **26,** 1–12.

Hasselmann, S., and K. Hasselmann, 1981: A symmetrical method of computing the nonlinear transfer in a gravity-wave spectrum. *Hamb. Geophys. Einzelschr.*, Ser. A, Wiss. Abh., **52,** 163 pp.

——, ——, J. H. Allender and T. P. Barnett, 1985: Computations and parameterizations of the nonlinear energy transfer in a gravity-wave spectrum. Part II: Parameterization of the nonlinear energy transfer for application in wave models. *J. Phys. Oceanogr.*, **15,** 1378–1391.

Hesselberg, Th., 1915: Über eine Beziehung zwischen Druckgradient, Wind und Gradientänderungen. *Veröff d. Geophysischen Inst.*, Ser. 2, Bd 1, 207–210.

Hino, M., M. Kashiwayanagi, A. Nakayama and T. Hara, 1983: Experiments on the turbulence statistics and the structure of a reciprocating oscillatory flow. *J. Fluid Mech.*, **131,** 363–400.

Janssen, P. A. E. M., G. J. Komen and W. J. P. de Voogt, 1984: An operational hybrid wave prediction model. *J. Geophys. Res.*, **89**(C3), 3635–3654.

Jonsson, I. G., 1980: A new approach to oscillatory rough turbulent boundary layers. *Ocean Eng.*, **7,** 109–152.

JONSWAP: Hasselmann, K., T. P. Barnett, E. Bouws, H. Carlson, D. E. Cartwright, K. Enke, J. A. Ewing, H. Gienapp, D. E. Hasselmann, P. Kruseman, A. Meerbrug, P. Müller, D. J. Olbers, K. Richter, W. Sell and H. Walden, 1973: Measurements of wind-wave growth and swell decay during the Joint North Sea Wave Project (JONSWAP). *Dtsch. Hydrogr. Z.*, (12), 95 p.

Kajiura, K., 1968: A model of the bottom boundary layer in water waves. *Bull. Earthquake Res. Inst.*, **46,** 75–123.

Karssen, B., 1987: Implementation of and first results with the NEDWAM model, a third-generation wave prediction model for the North Sea (in Dutch). KNMI Tech. Rep. TR-102, De Bilt, The Netherlands.

Kitaigorodskii, S. A., V. P. Krasitslii and M. M. Zaslavskii, 1975: On Phillips' theory of equilibrium range in the spectra of wind-generated gravity waves. *J. Phys. Oceanogr.*, **5,** 410–420.

Komar, P. D., R. H. Neudeck and L. D. Kulm, 1972: Observations and significance of deep-water oscillatory ripple marks on the Oregon continental shelf. *Shelf Sediment Transport: Process and Pattern,* D. G. P. Swift, D. D. Duana and O. H. Pilkey, Eds., Dowden, Hutchinson and Ross, 601–619.

Madsen, O. S., Y.-K. Poon and H. C. Graber, 1989: Spectral wave attenuation by bottom friction: theory. *Proc. 21st Int. Conf. Coastal Engineering,* Malaga, 492–504.

Phillips, O. M., 1980: *The Dynamics of the Upper Ocean,* 2nd ed. Cambridge University Press.

Schlichting, H., 1955: *Boundary Layer Theory.* McGraw Hill.

Shemdin, O., K. Hasselmann, S. V. Hsiao and K. Herterich, 1978: Nonlinear and linear bottom interaction effects in shallow water. *Turbulent Fluxes through the Sea Surface, Wave Dynamics, and Prediction,* Plenum, 647–665.

Sleath, J. F. A., 1984: Sea bed mechanics, Wiley Interscience.

Snyder, R. L., F. W. Dobson, J. A. Elliot and R. B. Long, 1981. Array measurements of atmospheric pressure fluctuations above surface gravity waves. *J. Fluid Mech.*, **102,** 1–59.

Soulsby, R. L., 1987: Calculating bottom orbital velocity beneath waves. *Coastal Eng.*, **11,** 371–380.

Sternberg, R. W., 1968: Friction factors in tidal channels with differing bed roughness. *Mar. Geol.*, **6,** 243–260.

SWIM: Bouws, E., J. J. Ephraums, J. A. Ewing, P. E. Francis, H. Günther, P. A. E. M. Janssen, G. J. Komen, W. Rosenthal and W. J. P. de Voogt, 1985: A shallow water intercomparison of wave prediction models (SWIM). *Quart. J. Roy. Meteor. Soc.,* **111,** 1087–1115.

Tolman, H. L., 1980: Wind wave propagation in tidal seas. PhD thesis. Rep. no. 90–1, Delft University of Technology, Delft, The Netherlands.

WAMDI group: Bauer, E., L. Bertotti, J. A. Ewing, J. A. Greenwood, A. Guillaume, K. Hasselmann, S. Hasselmann, P. A. E. M. Janssen, G. J. Komen, P. Lionello, M. Reistad and L. Zambresky, 1988: The WAM model—a third generation ocean wave prediction model. *J. Phys. Oceanogr.*, **18,** 1775–1810.

Weber, S. L., 1988: The energy balance of finite depth gravity waves. *J. Geophys. Res.*, **93,** 3601–3607.

Weber, S. L., 1989: Surface gravity waves and turbulent bottom friction. PhD thesis, University of Utrecht, The Netherlands.